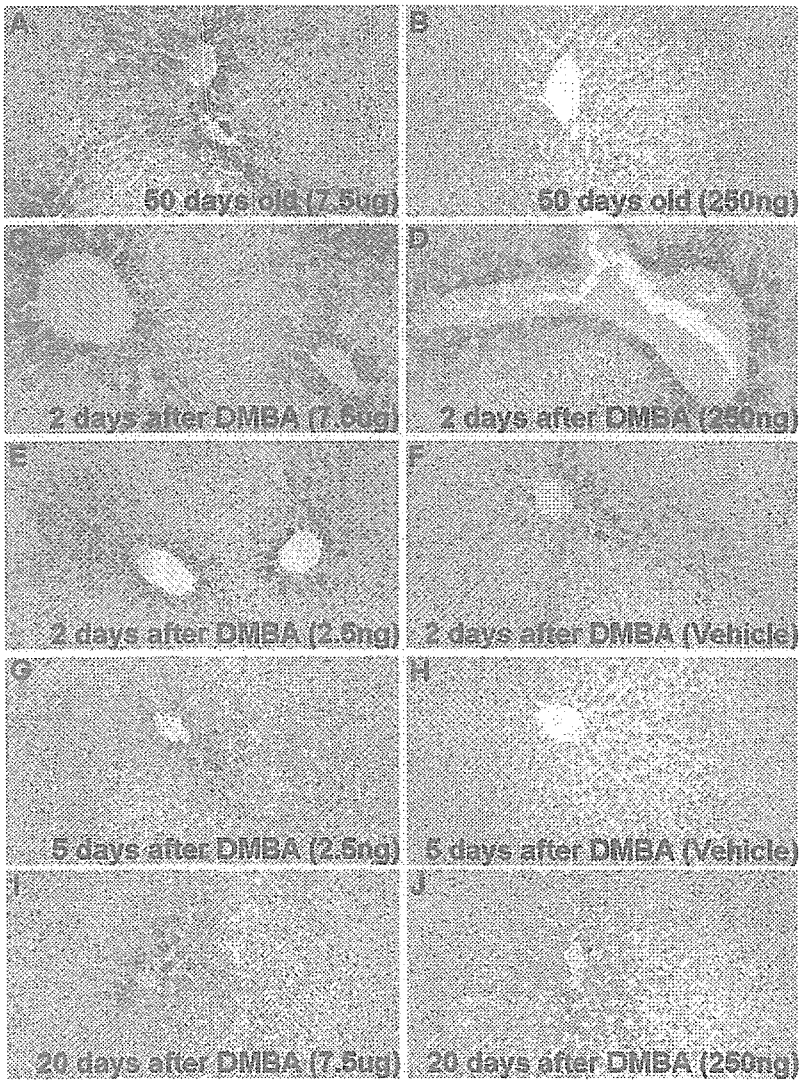

Fig. 6. Immunohistochemical analysis of CYP1A1 in rat liver. Just before DMBA ingestion, a large number of hepatocytes in the 7.5-μg group were positive (A) for CYP1A1, but negative in the 250-ng group (B). At 2 days after DMBA administration, a large number of hepatocytes were positive in the 7.5-μg (C) and 250-ng groups (D), and many hepatocytes were positive in the 2.5 ng (E) and vehicle groups (F). At 5 days after administration, some hepatocytes were positive in the 2.5-ng group (G), but none was positive in the vehicle group (H). At 20 days after DMBA administration, some hepatocytes were positive in the 7.5-μg group (I), and a few hepatocytes were positive in the 250-ng group (J). ABC method, Mayer's hematoxylin counterstain. Magnification ×140.

old. Because the 7.5-μg group possessed a high level of hepatic PCB126 residues (more than 31 times that of the other groups) on the day of DMBA ingestion, these CYP1 inductions were thought to be due to a complex induction by PCB126 residues and ingested DMBA, while the 250-ng and 2.5-ng group revealed prolonged CYP1 inductions compared to that of the vehicle group. Because the 250-ng and 2.5-ng groups showed a lower level of CYP1 with lower PCB126 residues at the time of DMBA ingestion (50 days old), it seems that prenatal exposure to PCB126 increases hepatocyte sensitivity in the rat for CYP1 induction by ingested DMBA.

The precise mechanism of the modulation of DMBA-induced mammary carcinogenesis by PCB126 remains to be explained, but one possible mechanism could be the ability of CYP1A1 and CYP1B1 to metabolize highly oxidative DMBA because carcinogenesis was dominant in the 250-ng group, while the concentration of PCB126 residues due to prenatal exposure that induced a high level of CYP1A1 was highest in the 7.5-μg group. The predominance of CYP1B1 in several human cancers, including breast carcinomas (Eltom et al., 1998; Merchant et al., 1993; Murray et al., 1997), has been reported. The functional involvement of CYP1B1 in PAH metabolism has been demonstrated by the fact that the metabolism of DMBA by microsomes from MCF-7 cells is inhibited by anti-CYP1B1 antibody, but not anti-CYP1A1 antibody (Christou et al., 1995). Although it is well known that PCBs specifically induce CYP1 (Angus et al., 1999; Christou et al., 1987; Tritscher et al., 1992), it remains to

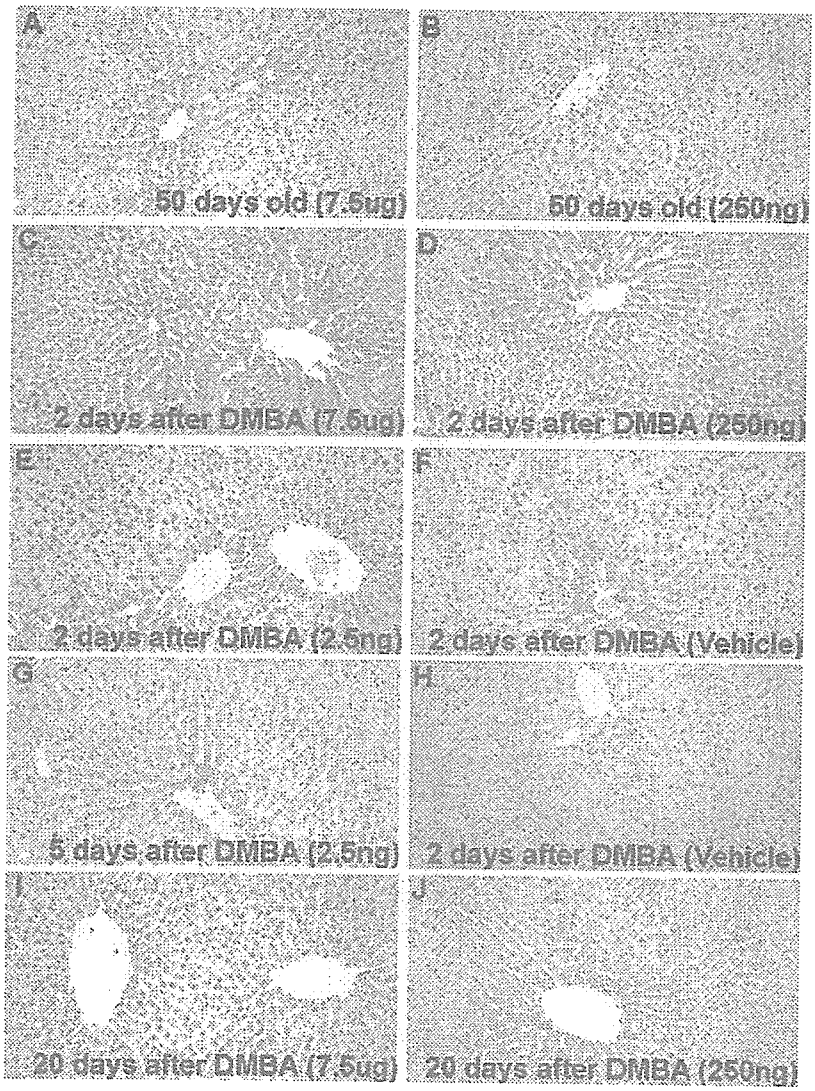

Fig. 7. Immunohistochemical analysis of CYP1B1 in rat liver. Just before DMBA ingestion, some hepatocytes in the 7.5-μg group were positive for CYP1B1 (A) but negative in the 250-ng group (B). At 2 days after DMBA administration, a large number of hepatocytes were positive in the 7.5-μg (C) and 250-ng groups (D), and many hepatocytes were positive in the 2.5 ng (E) and vehicle group (F). At 5 days after DMBA administration, some hepatocytes were positive in the 2.5 ng group (G), but none was positive in the vehicle group (H). At 20 days after DMBA administration, a few hepatocytes were positive in the 7.5-μg group (I), and some hepatocytes were positive in the 250-ng group (J). ABC method, Mayer's hematoxylin counterstain. Magnification ×140.

be determined why the 250-ng group showed higher CYP1B1 expression than the 7.5-μg group.

After DMBA was ingested to rats, previous studies have described the maximum urinary excretions of DMBA take place during the period ranging from 6 h to 1 day (Semin et al., 1976), and high levels of metabolite DMBA-DNA adducts in liver are found on days 1 to 2 (El-Bayoumy et al., 1992). Then, the large amounts of DMBA-DNA adducts in liver and mammary glands were remained to be observed at 12 days after DMBA ingestion (Daniel and Joyce, 1984), but their levels after that was unclear. Meanwhile, several previous studies have described the induction of rat hepatic CYP1 mRNA and/or protein within 1 day of DMBA ingestion (Badawi et al., 2000; Bolognesi et al., 1991; Granberg et al., 2000; Heidel et al., 1998; Moon et al., 1988; Rowlands et al., 2001). In our previous study, following DMBA ingestion without PCB126 exposure, the induction of hepatic CYP1A1 was first observed at 12 h, was revealed to peak on day 2 and decreased on day 5, and the induction of hepatic CYP1B1 was first observed on day 2 and decreased on day 5 (Muto et al., 2003). While present study revealed that prenatal PCB126 exposure rats were induced the prolongation of hepatic CYP1 induction following DMBA ingestion, especially the longer persistence of CYP1B1 induction was apparently in the 250-ng group. The implication of estradiol (E2) in breast tumorigenesis is widely documented (Nandi et al., 1995; Weinberg, 1996). An alternative mechanism of E2 carcinogenicity stems from the metabolism of this hormone, which generates several catechol derivatives from monohydroxylation reactions,

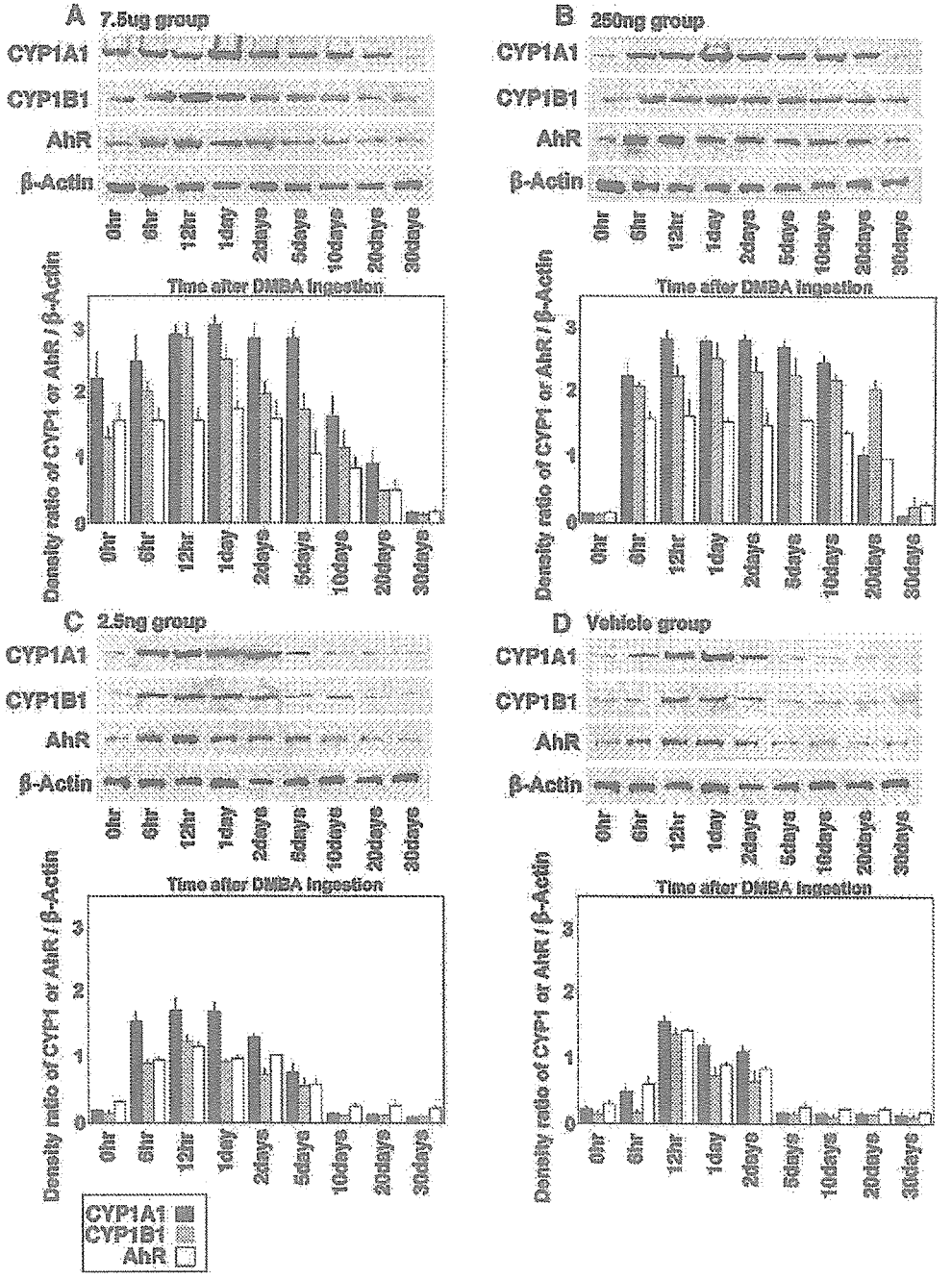

Fig. 8. Western blots of CYP1A1, CYP1B1, and AhR of rat liver following DMBA ingestion after prenatal exposure to PCB126. The protein concentration was determined with a bicinchonic acid protein assay reagent kit (Pierce) with bovine serum albumin as a standard. Ten μg of microsome samples were applied for Western blotting analysis, and immunoreactive proteins were detected using the ECL Plus Western Blotting Detection system (Amersham Biosciences, Buckinghamshire, UK). The upper panels show the representative Western blots bands of CYP1, AhR and β-actin, and the lower panels show the density ratio of CYP1, or AhR/β-actin: results are obtained by screening sample from five rats of each group. Values represent mean ± SD (A) the 7.5 μg group; (B) the 250 ng group; (C) the 2.5 ng group; (D) the vehicle group.

and liver is the primary site of E2 metabolism (Beleh et al., 1995; Waalkes et al., 2004; Wang and Liehr, 1994). This is in particular, the case of 4-hydroxylated E2, which is generated mainly by CYP1B1, displays a strong genotoxicity (Cavalieri et al., 2002; Safe and Krishnan, 1995). On the other hand, CYP1A1 generates primarily 2-hydroxylated E2, which is less toxic and has been considered as protective (Cavalieri et al., 2002; Liehr et al., 1995; Mobley et al., 1999; Schumacher et al., 1999; Yager and Liehr, 1996). Moreover, it has been suggested that the induction of mouse hepatic CYP1A1 is primarily protective for toxicity of DMBA (Uno et al., 2004). Therefore, it is possible that the prolongation of hepatic

CYP1B1 induction has been observed in the 250-ng group contributes to mammary carcinogenesis by bioactivation of both exogenous pro-carcinogens, DMBA, and endogenous E2.

A recent study showed elevated expression of AhR in the endometrium and myometrium (Khorram et al., 2002). In this study, the 250-ng group revealed elevated AhR expression compared to the other groups. Notably high levels of AhR in the liver of the 250-ng group suggest that elevated AhR expression mediated, at least in part, the increased expression of CYP1B1. As previously suggested, high levels of CYP1B1 expression, like hyperexpression of AhR, may represent a molecular marker for carcinogenesis (Spink et al., 1998). Moreover, AhR-deficient cells exhibit a decreased rate of cell proliferation because of a prolongation of cells in G1 (Ma and Whitlock, 1996; Weiss et al., 1996). The AhR also controls a number of genes whose products may be involved in a number of cellular proliferation and differentiation processes (Okey et al., 1994). In this study, because the 250-ng group showing enhancement of DMBA-induced mammary carcinogenesis revealed significantly higher AhR expression, AhR might mediate DMBA-induced mammary carcinogenesis through dysregulation of the cell cycle. However, it was unclear why a significantly lower induction of AhR was observed in the 7.5-μg group, which showed high-level PCB126 residues in mammary carcinomas, than in the 250-ng group.

Acknowledgments

The authors thank Ms. Katherine Ono for critical reading and editing of the manuscript. This study was supported by a Grant-in-Aid for High-Tech Research Center Project from the Ministry of Education, Science and Culture, Japan.

References

Angus, W.G., Larsen, M.C., Jefcoate, C.R., 1999. Expression of CYP1A1 and CYP1B1 depends on cell-specific factors in human breast cancer cell lines: role of estrogen receptor status. Carcinogenesis 20, 947–955.

Badawi, A.F., Cavalieri, E.L., Rogan, E.G., 2000. Effect of chlorinated hydrocarbons on expression of cytochrome P450 1A1, 1A2 and 1B1 and 2- and 4-hydroxylation of 17β-estradiol in female Sprague–Dawley rats. Carcinogenesis 21, 1593–1599.

Beleh, M.A., Lin, Y.C., Brueggemeier, R.W., 1995. Estrogen metabolism in microsomal, cell. and tissue preparations of kidney and liver from Syrian hamsters. J. Steroid Biochem. Mol. Biol. 52, 479–489.

Bolognesi, C., Parrini, M., Aiello, C., Rossi, L., 1991. DNA damage induced by 7,12-dimethylbenz[a]anthracene in the liver and the mammary gland of rats exposed to polycyclic aromatic hydrocarbon enzyme inducers during perinatal life. Mutagenesis 6, 113–116.

Bro-Rasmussen, F., 1996. Contamination by persistent chemicals in food chain and human health. Sci. Total Environ. 188, 45–60.

Burback, K.M., Poland, A.P., Bradfield, C.A., 1992. Cloning of the Ah receptor cDNA reveals a distinctive ligand-activated transcription factor. Proc. Natl. Acad. Sci. U.S.A. 89, 8185–8989.

Cavalieri, E.L., Balu, N., Saeed, M., Devanesan, P., 2002. Catechol ortho-quinones: the electrophilic compounds that form depurinating DNA adducts and could initiate cancer and other diseases. Carcinogenesis 23, 1071–1077.

Christou, M., Moore, C.J., Gould, M.N., Jefcoate, C.R., 1987. Induction of mammary cytochromes P-450: an essential first step in the metabolism of 7,12-dimethylbenz(*a*)anthracene by rat mammary epithelial cells. Carcinogenesis 8, 73–80.

Christou, M., Sava, U., Schroeder, S., Shen, X., Thompson, T., Gould, M., Jefcoate, C., 1995. Cytochromes CYP1A1 and CYP1B1 in the rat mammary gland: cell-specific expression and regulation by polycyclic aromatic hydrocarbons and hormones. Mol. Cell. Endocrinol. 115, 41–50.

Ciolino, H., Dankwah, M., Yeh, G., 2002. Resistance of MCF7 cells to dimethylbenz(*a*)anthracene induced apoptosis is due to reduced CYP1A1 expression. Int. J. Oncol. 21, 385–391.

Daniel, F.B., Joyce, N.J., 1984. 7,12-dimethylbenz[*a*]anthracene-DNA adduct in Sprague–Dawley and Long–Evans female rats. Carcinogenesis 5, 1021–1026.

Di Giovanni, J., Juchau, M.R., 1980. Biotransformation and bioactivation of 7,12-dimethylbenz[*a*]anthracene. Drug Metab. 11, 61–101.

Dipple, A., 1995. DNA adducts of chemical carcinogens. Carcinogenesis 16, 437–441.

Dipple, A., Moschel, R.C., Bigger, C.A.H., 1984. Polynuclear aromatic carcinogens. In: Earle, C.E.S. (Ed.), Chemical Carcinogens, 2nd ed. American Chemical Society, Washington, pp. 245–314.

Dipple, A., Khan, Q.A., Page, J.E., Ponten, I., Szeliga, J., 1999. DNA reactions, mutagenic action and stealth properties of polycyclic aromatic hydrocarbon carcinogenesis. Int. J. Oncol. 14, 103–111.

Dolwick, K.M., Schmidt, J.V., Carver, L.A., Swanson, H.J., Bradfield, C.A., 1993. Cloning and expression of a human Ah receptor cDNA. Mol. Pharmacol. 44, 911–917.

El-Bayoumy, K., Chae, Y.H., Upadhyaya, P., Meschter, C., Cohen, L.A., Reddy, B.S., 1992. Inhibition of 7,12-dimethylbenz[*a*]anthracene-induced tumors and DNA adduct formation in mammary glands of female Sprague–Dawley rats by the synthetic organoselenium compound, 1,4-phenylenebis[methylene]selenocyanate. Cancer Res. 52, 2402–2407.

Eltom, S., Larsen, M., Jefcoate, C., 1998. Expression of CYP1B1 but not CYP1A1 by primary cultured human mammary stromal fibroblasts constitutively and in response to dioxin exposure: role of the Ah receptor. Carcinogenesis 19, 1437–1444.

Evans, R.M., 1988. The steroid and thyroid hormone receptor superfamily. Science 240, 889–895.

Ginsberg, G.L., Atherholt, T.B., 1989. Transport of DNA-adducting metabolites in mouse serum following benzo(*a*)pryene administration. Carcinogenesis 10, 673–679.

Granberg, A.L., Brunstrom, B., Brandt, I., 2000. Cytochrome P450-dependent binding of 7,12-dimethylbenz[*a*]anthracene (DMBA) and benzo[*a*]pyrene (B[*a*]P) in murine heart, lung, and liver. Arch. Toxicol. 74, 593–601.

Heidel, S.M., Czuprynski, C.J., Jefcoate, C.R., 1998. Bone marrow stromal cells constitutively express high levels of cytochrome P4501B1 that metabolize 7,12 dimethlbenz[*a*]anthracene. Mol. Pharmacol. 54, 1000–1006.

Hoffman, E.C., Reyes, H., Chu, F.F., Sander, F., Conley, L.H., Brooks, B.A., Handkinson, O., 1991. Cloning of a factor required for activity of the Ah (dioxin) receptor. Science 252, 954–958.

Huggins, C., Grand, L.C., Brillantes, F.K., 1961. Mammary cancer induced by a single feeding of polynuclear hydrocarbons, and its suppression. Nature 189, 204–207.

IARC Working Group on the Evaluation of Carcinogenic Risks to Humans: Polychlorinated dibenzo-*para*-dioxins and polychlorinated dibenzofurans, 1997. IARC Monogr. Eval. Carcinog. Risks Hum. 69, 1–631.

Jones, P.B.C., Durrin, L.K., Galeazzi, D.R., Whilock, J., 1986. Control of cytochrome P-450 gene expression: analysis of a dioxin-responsive enhancer system. Proc. Natl. Acad. Sci. U.S.A. 83, 954–958.

Khorram, O., Gathwaite, M., Golos, T., 2002. Uterine and ovarian aryl

hydrocarbon receptor (AHR) and aryl hydrocarbon receptor nuclear translocator (ARNT) mRNA expression in benign and malignant gynecological conditions. Mol. Hum. Reprod. 8, 75–80.

Kothari, L., Subramanian, A., 1992. A possible modulatory influence of melatonin on representative phase I and II drug-metabolizing enzymes in 9,10-dimethyl-1,2-benzantracene-induced rat mammary tumorigenesis. Anti-Cancer Drugs 3, 623–928.

Kutz, F.W., Wood, P.H., Bottimore, D.P., 1991. Organochlorine pesticides and polychlorinated biphenyls in human adipose tissue. Rev. Environ. Contam. Toxiol. 60, 115–120.

Liehr, J.G., Ricci, M.J., Jefcoate, C.R., Hannigan, E.V., Hokanson, J.A., Zhu, B.T., 1995. 4-Hydroxylation of estradiol by human uterine myometrium and myoma microsomes: implications for the mechanism of uterine tumorigenesis. Proc. Natl. Acad. Sci. U.S.A. 92, 9220–9224.

Ma, Q., Whitlock, J.P., 1996. The aromatic hydrocarbon receptor modulates the Hepa 1c1c7 cell cycle and differentiated state independently of dioxin. Mol. Cell. Biol. 16, 2144–2150.

MacDonald, C.J., Cliolino, H.P., Yeh, G.C., 2001. Dibenzoylmethane modulates aryl hydrocarbon receptor function and expression of cytochromes P450 1A1 1B1. Cancer Res. 61, 3919–3924.

Merchant, M., Krishnan, V., Safe, S., 1993. Mechanism of action of alpha-naphthoflavone as an Ah receptor antagonist in MCF-7 human breast cancer cell. Toxicol. Appl. Pharmacol. 120, 53–63.

Mobley, J.A., Bhat, A.S., Bruggemeier, R.W., 1999. Measurement of oxidative DNA damage by catechol estrogens and analogues in vivo. Chem. Res. Toxicol. 12, 270–277.

Moon, C.J., Tricomi, W.A., Gould, M.N., 1988. Comparison of 7,12-dimethylbenz[*a*]anthracene metabolism and DNA binding in mammary epithelial cells from three rat strains with differing susceptibilities to mammary carcinogenesis. Carcinogenesis 9, 2099–2102.

Murphy, R., Harvey, C., 1985. Residues and metabolites of selected persistent halogenated hydrocarbons in blood samples from a general population survey. Environ. Health Perspect. 60, 115–130.

Murray, G.L., Taylor, M.C., McFadyen, M.C., MacKay, J.A., Greenlee, W.F., Burke, M.D., Melvin, W.T., 1997. Tumor-specific expression of cytochromes P450 CYP1B1. Cancer Res. 57, 3026–3031.

Muto, T., Wakui, S., Imano, N., Nakaaki, K., Hano, H., Furusato, M., Masaoka, T., 2001. In-utero and lactational exposure of 3,3′,4,4′,5-pentachlorobiphenyl modulate dimethylbenz[*a*]anthracene-induced rat mammary carcinogenesis. J. Toxicol. Pathol. 14, 213–224.

Muto, T., Watanabe, T., Moto, M., Okamura, M., Kashida, Y., Kanai, Y., Mitsumori, K., Endou, H., 2003. Time course of expression of 7,12-dimethylbenz[*a*]anthracene-induced CYP1A1 and CYP1B1 mRNA and protein in rat liver. J. Toxicol. Pathol. 16, 287–290.

Nandi, S., Guzman, R.C., Yang, J., 1995. Hormones and mammary carcinogenesis in mice, rat, and humans: a unifying hypothesis. Pro. Natl. Acad. Sci. U.S.A. 92, 3650–3657.

Okey, A.B., Riddick, D.S., Harper, P.A., 1994. The Ah receptor: mediator of the toxicity of 2,3,7,8-tetrachlorocibenzo-*p*-dioxin (TDCC) and related compounds. Toxicol. Lett. 70, 1–22.

Rogan, W.J., Gladen, B.C., McKinney, J.D., Carreras, N., Hardy, P., Thullen, J., Tigelstad, J., Tully, M., 1987. Polychlorinated biphenyls (PCBs) and dichlorodiphenyl dichloroethane (DDE) in human milk: effects on growth, morbidity and duration of lactation. Am. J. Publ. Health 77, 1294–1297.

Rowlands, J., He, L., Hakkak, R., Roins, M., Badger, T., 2001. Soy and whey proteins downregulate DMBA-induced liver and mammary gland CYP1 expression in female rats. Nutr. Cancer 131, 109–134.

Safe, S., Krishnan, V., 1995. Cellular and molecular biology of aryl hydrocarbon (Ah) receptor-mediated gene expression. Arch. Toxicol. 17, 99–115.

Sasaki, M., Kaneuchi, M., Fujimoto, S., Tanaka, Y., Dahiya, R., 2003. CYP1B1 gene in endometrial cancer. Mol. Cell. Endocrinol. 202, 171–176.

Schmidt, J., Bradfield, C., 1996. Ah receptor signaling pathways. Annu. Rev. Cell Dev. Biol. 12, 55–89.

Schumacher, G., Kataoka, M., Roth, J.A., Mukhopadhyay, T., 1999. Potent antitumor activity of 2-methoxyestradiol in human pancreatic cancer cell lines. Clin. Cancer Res. 5, 493–499.

Semin, B.K., Esakova, T.D., Petrusevich, I.M., Tarusov, B.N., 1976. Metabolism of 7,12-dimethylbenz(alpha)anthracene in vivo. Vopr. Onkol. 22, 54–58.

Shimada, T., Hayer, C., Yamazaki, H., Amin, S., Hecht, S., Guengerich, F., Sutte, T., 1996. Activity of chemically diverse precarinogens by human cytochrome P-450 1B1. Cancer Res. 56, 2979–2984.

Slaga, T.J., Gleason, G.L., DiGiovanni, J., Sukumaran, K.B., Harvey, R.G., 1979. Potent tumor-initiating activity of the 3,4-dihydrodiol of 7,12-dimethylbenz[*a*]anthracene in mouse skin. Cancer Res. 39, 1721–1723.

Slims, P., Grover, A., 1981. Involvement of dihydrodiols and dioepoxides in the metabolic activation of polycyclic hydrocarbons other than benzo[*a*]pyrene. In: Glboin, H.V., Ts'o, P.O.P. (Eds.), Polycyclic Hydrocarbons and Cancer, vol. 3. Academic Press, New York, NY, pp. 117–181.

Spink, D., Katz, B., Hussain, M., Pentecost, B., Cao, Z., Spink, C., 1998. Estrogen regulates Ah responsiveness in MCF-7 breast cancer cells. Carcinogenesis 24, 1941–1950.

Tanabe, S., Tatsukawa, R., Phillips, D., 1987. Mussels as bioindicators of PCB pollution: a case study on uptake and release of PCB isomers and congeners in green-lipped mussels (*Perna viridis*) in Hong Kong waters. Environ. Pollut. 47, 41–62.

Tritscher, A.M., Goldstein, J.A., Portier, C.J., McCoy, Z., Clark, G.C., Lucier, G.W., 1992. Dose-response relationships for chronic exposure to 2,3,7,8,-tetrachlorodibenzo-*p*-dioxin in a rat tumor promotion model: quantification and immunolocalization of CYP1A1 and CYP1A2 in the liver. Cancer Res. 52, 3436–3442.

Turteltaub, K.W., Felton, J.S., Gledhill, B.L., Vogel, J.S., Southon, J.R., Caffee, M.W., Finkel, R.C., Nelson, D.E., Procter, I.D., David, J.C., 1990. Accelerator mass spectrometry in biomedical dosimetry: relationship between low-level exposure and covalent binding of heterocyclic amine carcinogens to DNA. Proc. Natl. Acad. Sci. U.S.A. 87, 5288–5292.

Uno, S., Dalton, T.P., Derkenne, S., Curran, C.P., Miller, M.L., Shertzer, H.G., Nebert, D.W., 2004. Oral exposure to benzo[*a*]pyrene in the mouse: detoxication by inducible cytochrome P450 is more important than metabolic activation. Mol. Pharmacol. 65, 1225–1237.

van den Berg, M., Birnbaum, L., Bosveld, A.T.C., Brunstrom, B., Cook, P., Feely, M., Giesy, J.P., Hanberg, A., Hasegawa, R., Kennedy, S.W., Kubiak, T., Larsen, J.C., Rolaf van Leeuwen, F.X., Liem, A.K.D., Nolt, C., Peterson, R.E., Poellinger, L., Safe, S., Schrenk, D., Tillitt, D., Tysklind, M., Younes, M., Waern, F., Zacharewski, T., 1998. Toxic equivalency factors (TEFs) for PCBs, PCDDs, PCDFs for human and wildlife. Environ. Health Perspect. 106, 775–792.

Waalkes, M.P., Liu, J., Chen, H., Xie, Y., Achanzar, W.E., Zhou, Y.S., Cheng, M.L., Diwan, B.A., 2004. Estrogen signaling in livers of male mice with hepatocellular carcinoma induced by exposure to arsenic in utero. J. Natl. Cancer Inst. 96, 466–474.

Wang, M.Y., Liehr, J.G., 1994. Identification of fatty acid hydroperoxide cofactors in the cytochrome P450-mediated oxidation of estrogens to quinone metabolites. Role and balance of lipid peroxides during estrogen-induced carcinogenesis. J. Biol. Chem. 269, 284–291.

Weinberg, R.A., 1996. How cancer arises. Sci. Am. 275, 62–70.

Weiss, C., Kolluri, S.K., Kiefer, F., Gottlicher, M., 1996. Complementation of Ah receptor deficiency in hepatoma cells: negative feedback regulation and cell cycle control by Ah receptor. Ex. Cell Res. 226, 154–163.

Whitlock, J., 1999. Induction of cytochrome P4501A1. Annu. Rev. Pharmacol. Toxicol. 39, 103–125.

Yager, J.D., Liehr, J.G., 1996. Molecular mechanisms of estrogen carcinogenesis. Annu. Rev. Pharmacol. Toxicol. 36, 203–232.

Available online at www.sciencedirect.com
ScienceDirect
Biochimica et Biophysica Acta 1762 (2006) 673–682
BIOCHIMICA ET BIOPHYSICA ACTA
BBA
www.elsevier.com/locate/bbadis

Renal elimination of p-aminohippurate (PAH) in response to three days of biliary obstruction in the rat. The role of OAT1 and OAT3

Anabel Brandoni [a], Naohiko Anzai [b], Yoshikatsu Kanai [b], Hitoshi Endou [b], Adriana Mónica Torres [a,*]

[a] *Farmacología. Facultad de Ciencias Bioquímicas y Farmacéuticas. Universidad Nacional de Rosario. CONICET. Argentina*
[b] *Department of Pharmacology and Toxicology, Kyorin University School of Medicine, Tokyo, Japan*

Received 27 March 2006; received in revised form 24 May 2006; accepted 27 May 2006
Available online 7 June 2006

Abstract

Pharmacokinetic studies of the drugs administered to subjects with mechanical cholestasis are scarce. The purpose of the present study was to examine the effects of bile duct ligation of 3 days (peak of elevation of serum bile acids and bilirubin) on the systemic and renal PAH clearance and on the expression of cortical renal OAT1 and OAT3 in a rat model. PAH is the prototypical substrate of the renal organic anion transport system. Male Wistar rats underwent a bile duct ligation (BDL rats). Pair-fed sham-operated rats served as controls. BDL rats displayed a significantly lower systemic PAH clearance. Renal studies revealed a reduction in the renal clearance and in the excreted and secreted load of PAH in BDL rats. The OAT1 protein expression in kidney homogenates was not modified, but it decreased in the basolateral membranes from BDL rats. In contrast, OAT3 abundance in both kidney cortex homogenates and in basolateral membranes increased by 3 days after the ligation. Immunocytochemical studies (light microscopic and confocal immunofluorescence microscopic analyses) confirmed the changes in the renal expression of these transport proteins. The present study demonstrates the key role of OAT1 expression in the impaired elimination of PAH after 3 days of obstructive cholestasis.

Keywords: p-aminohippurate; Cholestasis; Renal depuration; OAT1; OAT3

1. Introduction

Extrahepatic, mechanical cholestasis occurs in about 10% of all patients suffering from cholelithiasis and in the majority of neoplasms affecting the pancreas and the common bile duct [1]. Prolonged cholestasis may alter the liver function due to an impaired uptake, changed biotransformation and secretion of compounds as well as secondary abnormalities induced within the kidney [2,3].

Pharmacokinetic studies of drugs administered to subjects with mechanical cholestasis are scarce [4]. Moreover, the obtained results are often conflicting, possibly due to the use of different species and interindividual differences.

The kidney and the liver play the major role in the elimination of numerous potentially toxic xenobiotics, including drugs, toxins, and endogenous metabolites. In some cases, the loss of one route of elimination can be compensated by the other [5]. It must also be mentioned that the impairment of liver or kidney functions can cause syndromes characterized by an injury of the alternative elimination organ [6,7].

In human beings and rats, extrahepatic cholestasis has been shown to render the kidney susceptible to a variety of nephrotoxic agents [6]. The pathophysiological cause of renal damage in the course of bile flow impairment is still not well understood, even though several phenomena, such as increased access of various constituents into the kidney (bilirubin and bile salts) have been suggested [6,7].

An impairment of the kidney function produces modifications in the renal elimination of drugs mediated by alterations in the blood flow to the kidney, glomerular filtration, active tubular secretion and passive tubular reabsorption [8].

The renal organic anion transport plays a critical role in protecting against the toxic effects of anionic substances, whether of

* Corresponding author. Suipacha 531, Rosario 2000, Argentina. Tel.: +54 341 4373787; fax: +54 341 4371992.
E-mail address: adtorres@fbioyf.unr.edu.ar (A.M. Torres).

0925-4439/$ - see front matter © 2006 Elsevier B.V. All rights reserved.
doi:10.1016/j.bbadis.2006.05.011

endogenous or environmental origin, by removing such substances from the blood principally via the organic anion transporter mechanisms found in the apical and basolateral membrane of renal epithelial cells. Several carrier proteins have been cloned and are functionally characterized from both membrane domains of rat kidneys [9–11]. The organic anion transporter 1 (OAT1) and the organic anion transporter 3 (OAT3) support the exchange organic anion/dicarboxylate transport in the basolateral membranes from the proximal tubule cells [12–15]. Two members of the multidrug resistance protein (MRP) family are located at the apical membranes from the proximal tubule cells, MRP2 and MRP4 [10,11,16,17]. The above mentioned four proteins mediate the renal transport of several anionic substances, such as p-aminohippurate (PAH), the prototypic organic anion commonly used in experimental studies. An up-regulation of renal MRP2 has been described at 1 and 3 days after bile duct ligation [18,19]. One day of bile duct ligation is referred as an early stage of obstructive cholestasis and 3 days of bile duct ligation is the period in which serum bile acids and bilirubin levels reach the peak of elevation [18–20]. MRP4 decreases at 3 days after bile duct ligation [21]. An increase in the urinary excretion of PAH has been concomitantly demonstrated with an increase in the abundance of OAT1 in the kidney homogenates in the early phase of an obstructive cholestasis [22].

The purpose of the present study was thus to examine the systemic and renal PAH clearance and the role of cortical renal OAT1 and OAT3 in response to 3 days of biliary obstruction in rats.

2. Materials and methods

2.1. Experimental animals

Male Wistar rats aged from 110 to 130 days old were used throughout the study (380–410 g body weight). In order to perform surgical procedures the animals were anaesthetized with sulfuric ether. After an upper abdominal incision was performed under sterile condition, the common bile duct was isolated and double-ligated close to the liver hilus immediately below the bifurcation and cut between the ligatures (BDL group). The controls then underwent a sham operation that consisted of exposure, but not a ligation, of the common bile duct (Sham group). The abdominal incision was then closed by single sutures. All studies were performed 3 days after surgery. All animals were allowed free access to a standard laboratory chow and tap water, and housed in a constant temperature and humidity environment with regular light cycles (12 h) during the experiment. All animals were cared for in accordance with the principles and guidelines for the care and use of laboratory animals [23].

2.2. Biochemical determinations

On the day of the experiment, blood was withdrawn from femoral artery of Sham and BDL animals. The serum was separated by centrifugation (3000 rpm, 3 min). These samples were used to measure total and direct bilirubin as parameters indicative of hepatic function and urea serum levels as a parameter indicative of global renal function. The above mentioned biochemical analyses were performed using optimized spectrophotometric techniques, while employing commercial kits (Wiener Laboratory).

2.3. Pharmacokinetic studies

These studies were done in a manner similar to those previously described [22,24]. At 3 days after surgery, the animals were anaesthetized with sodium thiopental (70 mg/kg b.w., i.p.). The femoral artery and the vein were both catheterized to obtain samples and to administer test compound, respectively. A single bolus of PAH (30 mg/kg b.w., aqueous solution, i.v.) was administered. Blood samples were obtained at 0–15 min range time after the administration of the PAH solution. The volume of blood samples was 50 μL. Eight blood samples were removed from each rat at different times between 0 and 15 min. An equivalent volume of isotonic saline solution was infused to restore the amount extracted in the blood samples. Samples were centrifuged at 3000 rpm for 3 min, and the extracted plasmas were frozen at −20 °C until analyzes.

At 15 min after PAH administration, a suprapubic incision was performed in order to isolate the bladder. Both ureters and the urethra were ligated with extreme care in order not to lose any urine. Thereafter, the bladder was removed and the whole contents of urine were then obtained to measure the quantity of PAH.

The plasma concentration vs. time curves for PAH, for each individual animal, were fitted with the PKCALC computer program [25]. The data were fitted to a biexponential curve. The choice of the best fit was based on the determination of coefficient values (R^2) and F test [25,26]. All fits had R^2 values >0.9. The following equation was used to describe the biexponential concentration–time curves:

$$Cp = Ae^{-\alpha t} + Be^{-\beta t}$$

where Cp is PAH plasma concentration (mg/mL) at time t (min) after administration; constant α represents the distribution from the central compartment and β is an equilibrium constant reflecting the dynamics between k_{21} and K_{10} and the slopes of each of the adjusted curves give their values. A and B represent the initial values of the distribution and elimination components, respectively, extrapolated from the y-axis intercept. The estimate parameters (α, β, A, B) were used to solve the first-order rate constants of transfer from the central to peripheral compartments (k_{12}, k_{21}) and the elimination rate constant from the central compartment (K_{10}) with classical equations. Derived parameters: area under curve (AUC), total volume of distribution (VdT), volume of the central compartment (VdC), volume of the peripheral compartment (VdP), steady-state volume of distribution (Vdss), systemic clearance (Cls), elimination half-life ($t_{1/2}$ β) were calculated according to standard procedures for the compartmental analysis. Cls was calculated as the Dose/AUC. The formulas for calculating the different volume of distribution were: VdT=Dose/[β×AUC], VdC=Dose/A+B, VdP=VdT−VdC, Vdss=Cls×MDRT, MDRT (mean disposition residence time)=AUMC/AUC, AUMC is the area under curve for the plot of the product of concentration and time vs. the time from time zero to infinity. Concentration of PAH in plasma and in urine was measured using the method described by Waugh and Beall [27].

2.4. Binding of PAH to plasma proteins

The binding of PAH to plasma proteins in Sham and BDL rats was determined using an ultrafiltration apparatus (Centrifree, Amicon, Millipore Corporation, Bedford, Mass) as previously described [24].

2.5. Renal excretion studies

These studies were performed as previously described [24,28–31]. Sham (n=4) and BDL (n=5) rats were anaesthetized as described. Femoral vein and artery were cannulated and a bladder catheter (3 mm i.d.) was inserted through a suprapubic incision. A priming dose of inulin (30 mg/kg b.w.) and PAH (30 mg/kg b.w.) in 1.5 mL of saline solution was administered through the venous catheter. Then, a solution containing inulin (12 g/L), PAH (12 g/L) and saline solution (9 g/L) was infused through the venous catheter employing a constant infusion pump (Pump 22; Harvard Apparatus, USA) at a rate of 1 mL/h/100 g b.w. After equilibrating for 45 min, urine was collected during two 20-min periods. Blood from the femoral artery was obtained at the midpoint of each clearance period. The arterial blood pressure was estimated throughout the experiments with a manometer inserted in the femoral artery. The glomerular filtration rate (GFR) was calculated from the clearance of inulin, in order to determine filtered load of PAH. The excreted, secreted and filtered loads of PAH were calculated by conventional formulae for each animal. The PAH concentrations in the serum and urine were determined by the method of Waugh and Beall [27] and the inulin concentrations were assayed by the procedure of Roe [32]. The volume of urine was determined by gravimetry.

2.6. Preparation of basolateral membrane (BLM) from kidney cortex

The preparations of BLM from Sham and BDL rats were done by a modification of the method described by Jensen and Berndt [33] as previously reported by

us [24,29]. Kidney cortical tissues were placed in a Dounce homogenizer containing 250 mM sucrose, 5 mM Tris–HEPES pH 7.40 at a ratio of 12.5 mL/g cortex wet weight. After four gentle strokes with the loose fitting pestle, the suspension was homogenized further with a motor-driven teflon pestle (600 rpm/5 strokes) and spun down for 15 min at 1200×*g*. The supernatant was aspirated and spun for 15 min at 22,000×*g*. The fluffy beige upper layer of the resulting pellet (crude plasma membranes) was resuspended in about 1 mL of supernatant and added to 19 mL of buffered sucrose. The membrane suspension was homogenized gently through a 16-gauge gavage needle followed by the addition of 3.7 mL of 100% Percoll. The Percoll-membranes mixture was spun for 30 min at 39,250×*g*. The top clear layer was discarded and the top-most dark band was removed. This layer was composed primarily of basolateral membranes. BLM were brought up in KCl buffer (85 mM KCl, 83 mM sucrose, 2 mM HEPES–Tris pH 7.40) at a ratio of 8 mL/g original cortex wet weight. Next, BLM were pelleted at 30,000×*g* for 30 min and washed three times with the KCl buffer. Finally, BLM were resuspended in 300 μL of 250 mM manitol, 10 mM HEPES–Tris, pH 7.40. Aliquots of the membranes were stored immediately at −70 °C until use (no more than 2 weeks after membrane preparations). Each preparation represents cortical tissue from four animals. Four preparations were obtained for each experimental group. Protein quantification of samples was performed using the method of Sedmak and Grossberg [34].

2.7. Electrophoresis and immunoblotting

Homogenates and basolateral membranes were boiled for 3 min in the presence of 1% 2-mercaptoethanol/2% SDS (Sodium Dodecyl Sulphate). Samples were applied to a 8.5% polyacrilamide gel, separated by SDS-PAGE, and then electroblotted to nitrocellulose membranes. Membranes were stained with Ponceau Red to confirm equal protein loading and transfer between lanes as previously described [21,22,28–30]. The nitrocellulose membranes were incubated with 5% nonfat dry milk in phosphate-buffer saline containing 0.1% Tween 20 (PBST) for 2 h. After being rinsed with PBST, the membranes were then incubated overnight at 4 °C with a commercial rabbit polyclonal antibody against rat OAT1 (1.25 μg/mL) and with commercial mouse monoclonal antibody against human β-Actin (1.25 μg/mL) or with non-commercial rabbit polyclonal antibody against rat OAT3 (at a dilution of 1:1000) and with commercial mouse monoclonal antibody against human β-Actin (1.25 μg/mL). The specificity of OAT3 antibody has been described elsewhere [15]. The membranes were incubated for 1 h with a peroxidase coupled goat anti-rabbit IgG (Bio-Rad) or with a peroxidase coupled sheep anti mouse IgG (Amersham) after further washing with PBST. Blots were processed for detection using commercial kit (Opti-4CN, Bio-Rad for OAT1 and ECL enhanced chemiluminescence system, Amersham for OAT3). To investigate the specificity of the bands, an absorption test was performed. The OAT1 peptide (1.25 μg/mL) or OAT3 peptide (0.50 mg/mL) were added to the OAT1-antibody specific solution or OAT3-antibody specific solution respectively and incubated for 2 h. Using these preabsorbed antibodies, Western blot analyses were performed as described above. A densitometric quantification of the Western blot signal intensity of membranes was performed.

Table 1
Pharmacokinetic parameters of PAH in Sham ($n=7$) and BDL ($n=8$) rats after a single dose (30 mg/kg b.w., i.v.)

	Sham	BDL
AUC (mg/min/mL)	0.88±0.04	1.34±0.15*
Cls (mL/min/100 g b.w.)	3.46±0.21	2.44±0.25*
A (mg/mL)	0.207±0.016	0.205±0.021
B (mg/mL)	0.095±0.016	0.087±0.013
α (min^{-1})	1.35±0.11	0.82±0.07*
β (min^{-1})	0.128±0.012	0.083±0.008*
K_{10} (min^{-1})	0.345±0.017	0.234±0.022*
k_{12} (min^{-1})	0.612±0.062	0.378±0.064*
K_{21} (min^{-1})	0.523±0.086	0.289±0.024*
$t_{1/2}$ (β) (min)	5.67±0.48	8.88±0.85*
VdT (mL/100 g b.w.)	28.43±2.79	31.12±4.37
VdC (mL/100 g b.w.)	10.11±0.55	10.50±0.59
VdP (mL/100 g b.w.)	18.32±2.52	20.61±4.16
Vdss (mL/100 g b.w.)	23.29±1.92	25.16±3.47

The results are expressed as the means±SEM. (*) $P<0.05$.
AUC=area under curve; Cls=systemic clearance; constant α represent the distribution from the central compartment and β is an equilibrium constant reflecting the dynamics between k_{21} and K_{10}; A and B represent the initial values of the distribution and elimination components, respectively; K_{10}=elimination constant from the central compartment; $t_{1/2}(\beta)$=elimination half-life ($t_{1/2}$); VdT=total volume of distribution; VdC=volume of the central compartment; VdP=volume of the peripheral compartment; Vdss=steady-state volume of distribution.

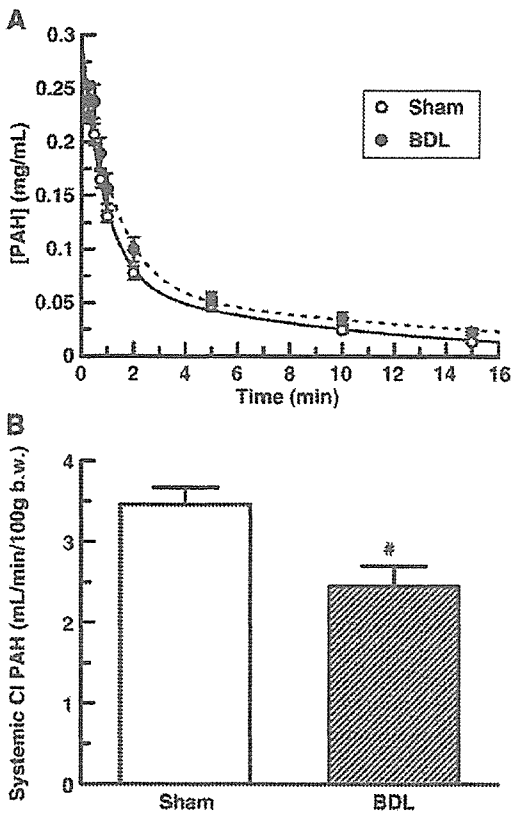

Fig. 1. Mean plasma concentration-time profile of PAH (A) and Systemic clearance of PAH (B) in Sham ($n=7$) and BDL ($n=8$) rats following a single 30 mg/kg b.w., i.v. dose of PAH. Results are expressed as the means±SEM. #$P<0.05$.

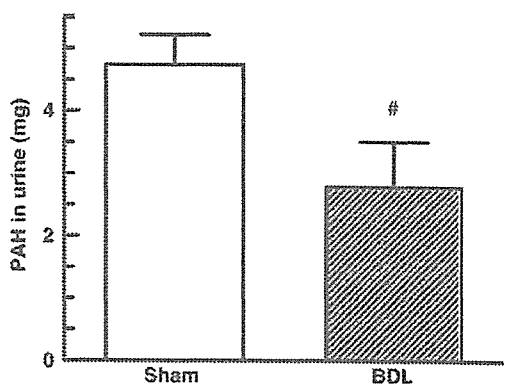

Fig. 2. Amount of PAH in urine excreted during 15 min following a single dose of PAH (30 mg/kg b.w., i.v.) in Sham ($n=7$) and BDL ($n=8$) animals. Results are expressed as the means±SEM. #$P<0.05$.

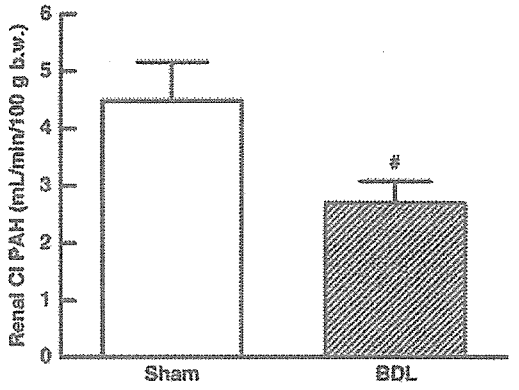

Fig. 3. Renal clearance of PAH in Sham ($n=4$) and BDL ($n=5$) rats. Results are expressed as the means±SEM. $^{\#}P<0.05$.

2.8. Immunocytochemistry microscopy

Kidneys from Sham and BDL rats were briefly perfused with saline, followed by perfusion with periodate–lysine–paraformaldehyde solution (0.01 M $NaIO_4$, 0.075 M lysine, 0.0375 M phosphate buffer, with 2% paraformaldehyde, pH: 6.20), through an abdominal cannula. The kidneys slices were immersed in periodate–lysine–paraformaldehyde solution at 4 °C overnight. The tissue was embedded in paraffin. Paraffin sections were cut. After deparaffining, the sections were incubated with 3% H_2O_2 for 15 min (to eliminate endogenous peroxidase activity) and then with blocking serum for 30 min. The sections were then incubated with non-commercial polyclonal antibodies against OAT1 (diluted 1:1000) or OAT3 (diluted 1:1000) overnight at 4 °C. The specificity of both antibodies has been described elsewhere [15]. The sections were rinsed with PBST.

2.9. Light microscopic analysis

The sections were incubated with biotinylated secondary antibody against rabbit Immunoglobulin for 1 h (biotinylated Ig Multi-Link Biogenex). After being rinsed with PBST, the sections were incubated for 30 min with horseradish peroxidase (HRP)-conjugated streptavidin solution (Streptavidin/HRP complex Multi-Link Biogenex). In order to detect HRP labeling a peroxidase substrate solution with diaminobenzidine (0.05% diaminobenzidine in PBST with 0.05% H_2O_2) was used. The sections were counterstained with hematoxylin before being examined under a light microscope.

2.10. Confocal microscopic analysis

The sections were incubated with Alexa 488 fluorochrome-conjugated goat anti-rabbit IgG, 1:1000 (Molecular Probes, Eugene, OR) overnight at 4 °C. Sections were washed with PBST and then mounted. Afterwards, they were viewed on a Zeiss Axiophot microscope equipped with an epifluorescence detector and a Bio-Rad MRC 1260 confocal imaging system.

Controls using preimmune serum, antiserum absorbed with excess synthetic peptide (as described above), or omission of primary or secondary antibody revealed no labeling.

Table 2
Body weight, kidneys weight, kidney/body weight ratio, plasma PAH concentrations (P_{PAH}), glomerular filtration rate (GFR), filtered, secreted and excreted loads of PAH (FL_{PAH}, SL_{PAH}, EL_{PAH}) in Sham ($n=4$) and BDL ($n=5$) rats

	Sham	BDL
Body weight (g)	342±18	367±7
Kidneys weight (g)	2.34±0.16	2.57±0.09
Kidney/Body weight ratio ($\times 10^{-3}$)	6.84±0.26	6.99±0.16
P_{PAH} (μM)	295±28	376±63
GFR (mL/min/100 g b.w.)	0.858±0.074	0.515±0.058*
FL_{PAH} (μg/min/ 100 g b.w.)	40±4	35±5
SL_{PAH} (μg/min/ 100 g b.w.)	169±10	140±6*
EL_{PAH} (μg/min/100 g b.w.)	209±13	175±10*

The results are expressed as the means±SEM.
* $P<0.05$.

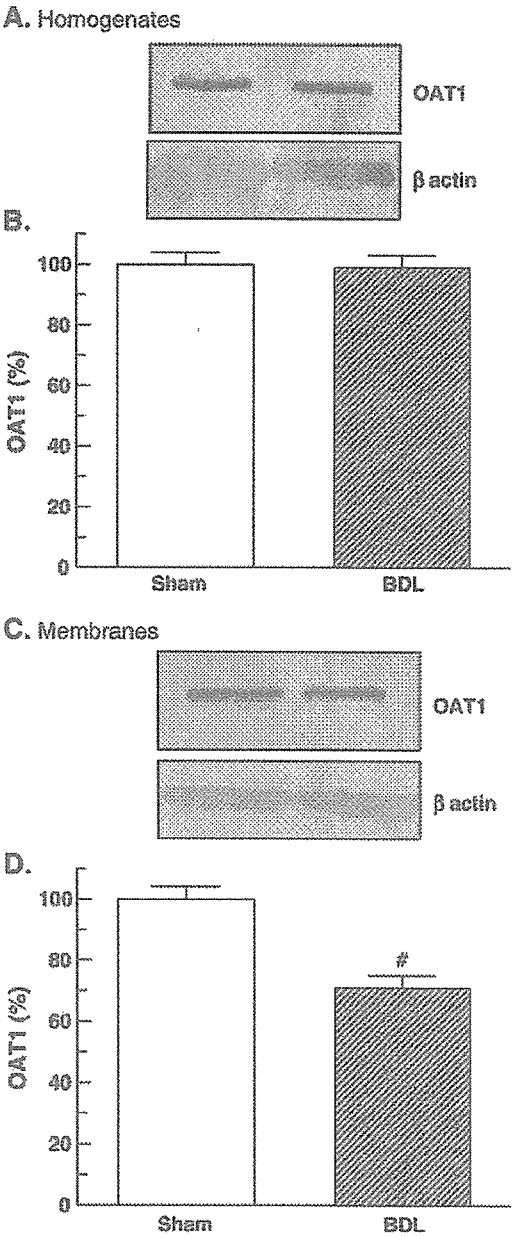

Fig. 4. Renal homogenates (50 μg proteins) (A) and basolateral membranes (40 μg proteins) (C) from kidneys of Sham and BDL rats were separated by sodium docecyl sulphate-polyacrylamide gel electrophoresis (8.5%) and blotted onto nitrocellulose membranes. OAT1 was identified using commercial polyclonal antibodies as described in Materials and methods. Densitometric quantification of OAT1 Western immunoblotting from renal homogenates (B) and basolateral membranes (D). The results are expressed as percentage, normalized for the β actin density. The Sham levels were set at 100%. Each column represents the mean± SEM from experiments carried out in four different preparations for each experimental group. $^{\#}P<0.05$.

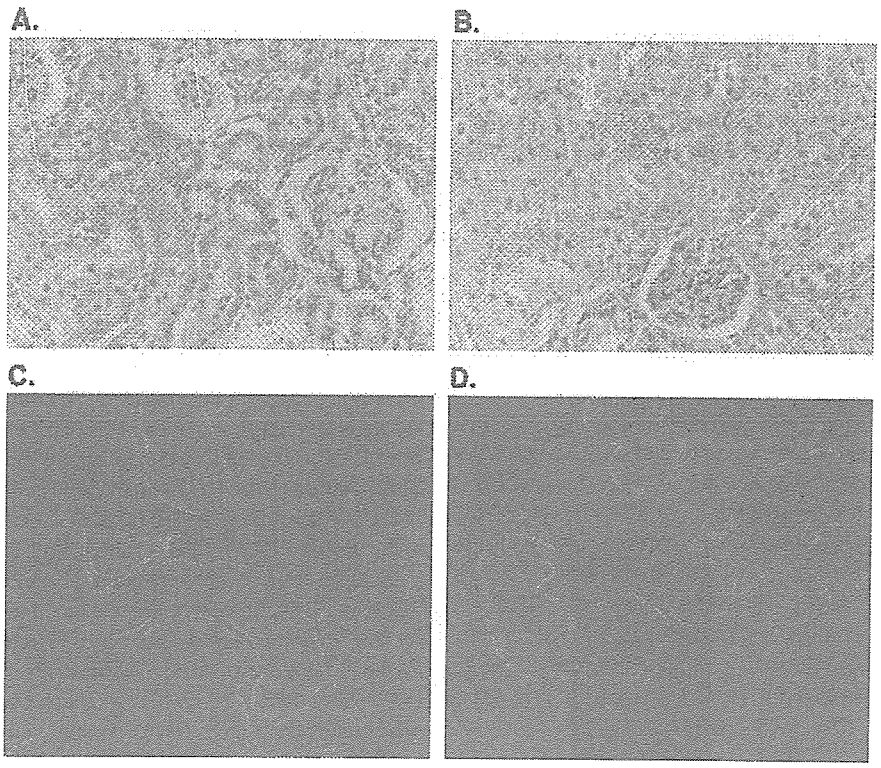

Fig. 5. Immunocytochemistry for OAT1. (A and B) Immunoperoxidase in the renal cortex of Sham (A) and BDL rats (B). Serial sections from each rat kidney were stained using a non-commercial anti-rOAT1 antibody (crude immune serum). OAT1 labeling was seen at the basolateral domains of proximal tubule cells. In BDL rats, it can be seen that OAT1 labeling in BLM is greatly reduced. These figures are representative of typical samples from four rats. Magnification ×400. (C and D) Immunofluorescence localization of OAT1 in the renal cortex of Sham (C) and BDL rats (D). Serial sections from each rat kidney were stained using a non-commercial anti-rOAT1 antibody (crude immune serum). In BDL rats, it can be seen OAT1 labeling throughout the cytoplasm in the proximal tubules, whereas the labeling of BLM was greatly reduced. These figures are representative of typical samples from four rats. Magnification ×400.

2.11. Histopathological studies

Histopathology of kidneys was performed after fixing in 10% neutral buffered formaldehyde solution for 4 h and embedding in paraffin, then 4 μm thick sections were processed for routine staining with hematoxylin and eosin, or stained with hematoxilin and PAS.

2.12. Materials

Chemicals were purchased from Sigma (St. Louis, MO, USA) and were analytical grade pure. The polyclonal antibodies against OAT1, monoclonal antibodies against β-actin and the OAT1 peptide for Western blotting were purchased from Alpha Diagnostic International (San Antonio, TX, USA). The polyclonal antibody against OAT1 for immunocytochemical studies and polyclonal antibody against OAT3 and the OAT3 peptide for both Western and immunocytochemical studies were non-commercial [15].

2.13. Statistical analysis

The statistical analysis was performed using the unpaired *t*-test. When variances were not homogeneous a Welch's correction was employed. *P* values of less than 0.05 were considered significant. The values are expressed as the means ± standard error (SEM). For these analyses, a GraphPad software was used. For densitometry of immunoblots, samples from kidneys of BDL rats were run on each gel with corresponding Sham kidneys. The abundance of OAT1 and OAT3 in the samples from the experimental animals was calculated as percentage of the mean Sham control value for that gel.

3. Results

Total bilirubin concentration in BDL rats increased to 71.34 ± 4.31 mg/L from 2.51 ± 0.36 mg/L observed in Sham group, whereas direct bilirubin level increased from 1.30 ± 0.24 mg/L in Sham animals to 66.85 ± 4.16 mg/L in BDL ones. Light microscopy only showed significant renal morphological alterations in PAS stained kidneys. In BDL rats, the kidney appears congestive, predominantly in the medulla. The tubular epithelium is less tall and shows apical extrusions and its foldings are less conspicuous. The cytoplasm presents a PAS (+) granularity. The tubules are moderately dilated, containing intraluminal proteinaceous, eosinophilic and acidophylic, material. These results are similar to those described by Wójcicki et al. [4].

On the other hand, no significant difference in the urea serum levels (g/L) was observed between the Sham-operated and BDL animals (0.40 ± 0.02 vs. 0.41 ± 0.02 respectively).

The mean plasma concentration-time profiles for PAH in Sham and BDL rats are shown in Fig. 1A. The higher plasma concentrations of PAH in BDL group were displayed during the distribution and elimination phases. BDL rats displayed a significant higher area under the curve and therefore a significant lower systemic clearance for PAH (Fig. 1B). The constant α (which represents the distribution from the central compartment),

the constant β (which is an equilibrium constant reflecting the dynamics between k_{21} and K_{10}), the rate constants of transfer from central to peripheral compartments (k_{12}, k_{21}) and the elimination rate constant from the central compartment (K_{10}) were all decreased in BDL rats, thus indicating the impairment in the rates of distribution and elimination of PAH (see Table 1). The distribution volumes were not significantly different between the Sham-operated and BDL animals as it is shown in Table 1.

A statistically significant decrease was observed in the quantity of PAH excreted in urine during 15 min (Fig. 2).

The percentage of unbound PAH to plasma proteins was higher in BDL rats than in the Sham ones (100±0.1 (n=4) vs. 95.3±1.4 (n=4), P<0.05, respectively). The values obtained for the Sham rats are similar to those previously reported [24].

Renal studies showed a decrease in the renal clearance of PAH in BDL rats as it is shown in Fig. 3. The excreted, secreted and filtered loads of PAH were lower in BDL rats compared with Sham rats, even though for the filtered load of PAH the difference did not reach the level of significance (Table 2). The glomerular filtration rate from jaundiced group was significantly lower in comparison with Sham group as it is also shown in Table 2. As a result, excreted load of PAH was lower in the BDL rats as consequence of the decrease in the secreted load of this organic anion.

Kidney cortex homogenates and basolateral membranes from Sham and BDL animals were subjected to immunoblot analyses for OAT1 protein. Fig. 4 shows no difference between the groups in the homogenates OAT1 expression. On the other hand, a lower abundance of OAT1 was observed in the basolateral membranes from BDL rats in comparison to the Sham rats. The OAT1 protein disappeared when the antibody was preabsorbed to the synthetic antigen peptide (data not shown).

Immunocytochemistry using horseradish peroxidase-conjugated secondary antibodies for light microscopy confirmed the reduced OAT1 expression in basolateral plasma membranes from BDL rats (Fig. 5B). The Sham rats showed an abundant OAT1 labeling in basolateral domains (Fig. 5A). To further characterize the distribution of OAT1 labeling in the proximal tubule cells, immunofluorescence was used (Fig. 5C and D). Confocal immunofluorescence studies also revealed a decrease in OAT1 labeling in basolateral plasma membranes and allowed a better appreciation of a punctuate labeling for OAT1, which was distributed widely throughout the cytoplasm in the kidneys from the BDL rats demonstrating the cellular internalization of this carrier protein.

The Western blotting findings of the kidney cortex homogenates and BLM from Sham and BDL rats showed signals for OAT3. In Fig. 6 it is possible to observe that the OAT3 abundance significantly increased in the kidney cortex homogenates and in the BLM from BDL rats in comparison to Sham ones. These signals were not observed when the antibody was preabsorbed with the OAT3 peptide (data not shown).

Immunocytochemistry studies showed staining for OAT3 in many parts of the nephron such as the proximal tubule (S1, S2 and S3), the distal and the collecting duct as it has been previously described [15]. Sham rats showed OAT3 labeling in basolateral membrane domain and inside the cytoplasm of renal tubular cells (Fig. 7A). Increased labeling was seen in the basolateral membranes of the tubules from kidneys of BDL rats (Fig. 7B). Immunofluorescence microscopy showed the basolateral membrane localization of OAT3 and a better detection of the intracellular localization (Fig. 7C). An important increase of OAT3 in basolateral membranes was observed in the cortex from

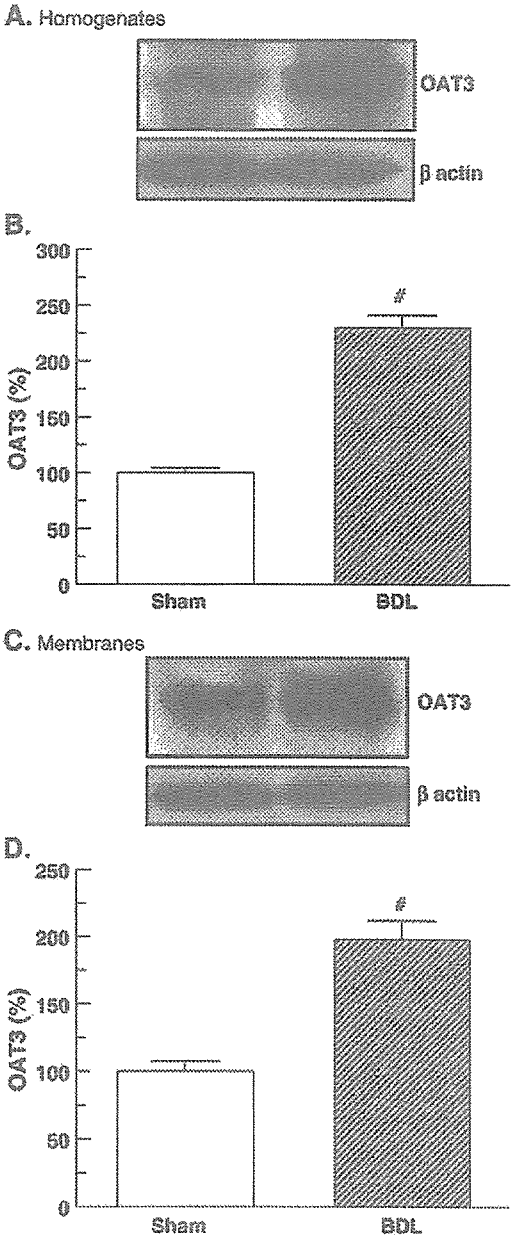

Fig. 6. Renal homogenates (50 μg proteins) (A) and basolateral membranes (40 μg proteins) (C) from kidneys of Sham and BDL rats were separated by sodium docecyl sulphate-polyacrylamide gel electrophoresis (8.5%) and blotted onto nitrocellulose membranes. OAT3 was identified using non-commercial polyclonal antibodies as described in Materials and methods. The densitometric quantification of the OAT3 Western immunoblotting from renal homogenates (B) and basolateral membranes (D). Results are expressed as percentage, normalized for the β actin density. The Sham levels were set at 100%. Each column represents the mean±SEM from experiments carried out in four different membrane preparations for each experimental group. $^{\#}P$<0.05.

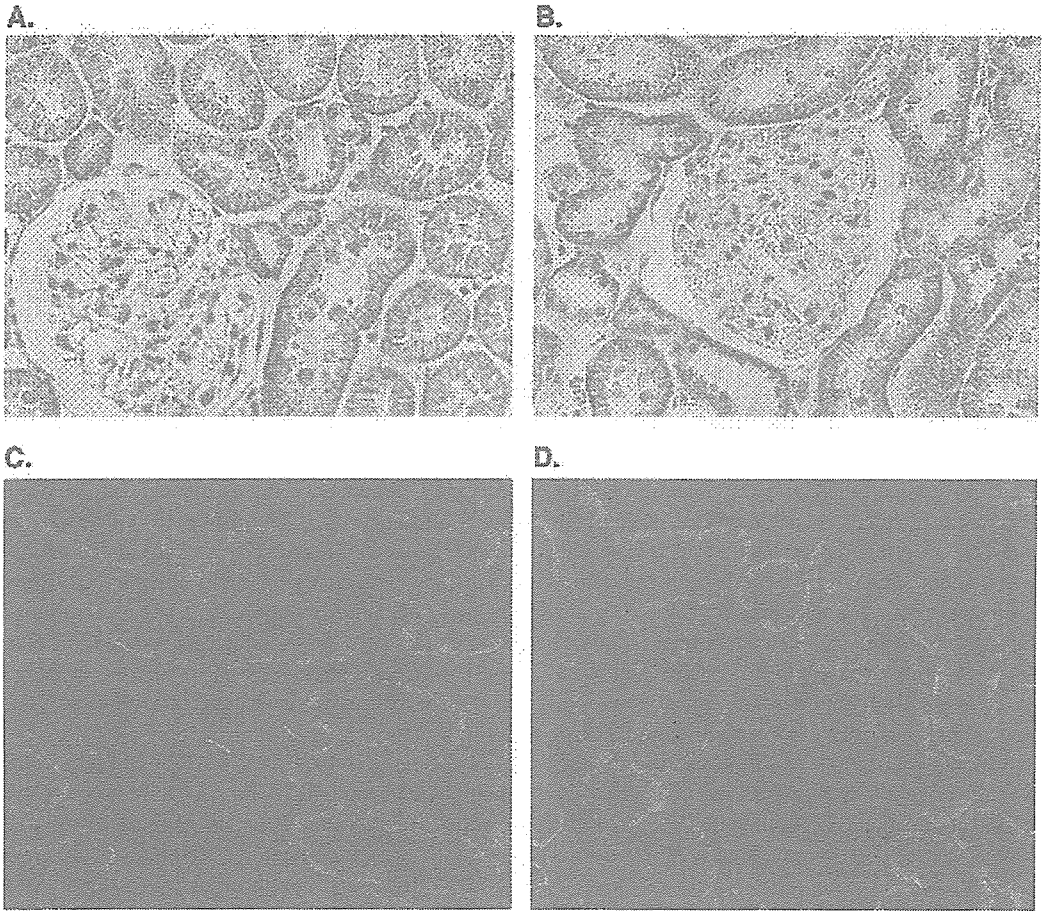

Fig. 7. Immunocytochemistry for OAT3. (A and B) Immunoperoxidase in the renal cortex of Sham (A) and BDL rats (B). Serial sections from each rat kidney were stained using a non-commercial anti-rOAT3 antibody. OAT3 labeling was seen at the basolateral domains of tubule cells and inside the cells. In BDL rats, it can be seen an increased OAT3 labeling in BLM. These figures are representative of typical samples from four rats. Magnification ×400. (C and D) Immunofluorescence localization of OAT3 in the renal cortex of the Sham (C) and BDL rats (D). Serial sections from each rat kidney were stained using a non-commercial anti-rOAT3 antibody. OAT3 labeling was seen at the basolateral domains of tubule cells and inside the cells. In the BDL rats, it could be seen as an increased OAT3 labeling in the BLM of tubular cells. These figures are representative of typical samples from four rats. Magnification ×400.

kidneys of BDL rats (Fig. 7D). This pattern parallels the data from an immunoblotting study.

4. Discussion

A large and diverse number of organic anions, or weak organic acids that exist as anions at physiological pH, are secreted by mammalian renal tubules. Substrates for the renal organic anion transport system include weak acids that have a net negative charge on carboxyl or sulfonyl residues at physiological pH [9–11]. Although this system secretes a number of endogenous compounds, it is generally accepted that is particularly important in secreting numerous exogenous compounds, including pharmacologically active substances, industrial and environmental toxins, and plant and animal toxins [9–11]. The transport of these substances across the basolateral membrane of renal epithelial cells is energetically uphill [9–11]. Molecular candidates for each of the organic anion transport process have been cloned, including OAT1 and OAT3 that serve as organic anion/dicarboxylate exchangers at the basolateral membrane of renal proximal tubule cells [9–15]. An unexplored aspect of OATs regulation concerns the body's response to disease states. We have recently demonstrated alterations in renal OAT1 and OAT3 expression in different experimental models in rats such as bilateral ureteral obstruction [28,29], arterial calcinosis [31], and chronic renal failure [30]. However, little is known about the regulation of these transporters after the early phase of extrahepatic cholestasis.

Acute jaundice due to bile duct obstruction is defined as the retention of bile and bile components. Biliary excretion of organic anions is a critical physiologic function of the liver. However, in obstructive jaundice, in which the biliary transport is impaired, adaptive mechanisms involving protein expression may permit urinary excretion of those potentially toxic compounds [1,4]. There are limited data on the pharmacokinetics of drugs in subjects with biliary obstruction.

Performing bile duct ligation as a well-established model of cholestasis, we have determined an increase in the systemic clearance of PAH associated to an increase in the abundance of OAT1 in renal cortex homogenates in rats at 21 h after bile duct ligation (early phase of acute extrahepatic cholestasis) [22]. The

aim of the present study was to examine the systemic and the renal clearance of PAH and the expression of both OAT1 and OAT3 in homogenates and basolateral membranes from rat renal cortex after a period of 3 days of bile duct obstruction (it has been well documented that serum bile salts and bilirubin levels reach the peak of elevation after 3 days of ligation [18–20]).

The clearance of a drug may be defined in a general way as "a proportionality constant describing the relationship between a substance's rate of transfer, in amount per unit time, and its concentration, in an appropriate reference fluid" [35]. The current study shows that rats at 3 days after bile duct ligation exhibit an increase in the area under the PAH plasma concentration–time curve and therefore, a statistically different decrease in the total body clearance. Furthermore, the total body clearance can be expressed as the product of the elimination rate microconstant ($K_{1\text{-}0}$) from the central compartment and the volume of such compartment. This last parameter was not modified in rats with extrahepatic cholestasis. On the other hand, a decrease was observed in $K_{1\text{-}0}$ in bile duct ligated rats as compared with Sham ones. $K_{1\text{-}0}$ is influenced by variables that participate in the elimination of the drug from the central compartment, such as metabolization, renal and biliary excretion. As PAH metabolization and biliary excretion is negligible, the decrease of $K_{1\text{-}0}$ observed in treated animals indicates a lower renal elimination of this organic anion. In this connection, rats subjected to bile duct ligation for 3 days showed a diminished renal PAH clearance. The decrease in renal PAH elimination is accounted for the diminished secreted load of the drug, since the filtered load of PAH was not modified in the BDL group.

In this cholestatic model, the OAT1 expression significantly decreased in the basolateral membranes from kidneys after 3 days of bile duct ligation. In addition to immunoblotting, immunocytochemical techniques corroborates the decrease in the basolateral membranes expression of OAT1 together with a significantly enhanced immunocytochemical staining for OAT1 in the cytoplasm of proximal tubule cells of BDL kidneys, which might suggest an internalization of membrane transporters or an inhibition in the recruitment of preformed transporters into the membranes.

It has been demonstrated that OAT1, when heterologously expressed in oocytes or mammalian cells, is inhibited by more or less selective PKC activators [36,37]. In this connection, it was demonstrated by Wolff et al. [38] that PKC induces human OAT1 down-regulation through carrier retrieval from the cell membrane and it does not involve phosphorylation. It is well known that angiotensin II [39] modulates the renal proximal tubule function via activation of PKC. Although the role of the renin–angiotensin system in the BDL model remains controversial [7], some humoral factors including angiotensin II induced by the 3 days BDL may induce the activation of PKC. Moreover, bile acids and high bilirubin levels can activate PKC [40,41]. It has been demonstrated that 3 days of bile duct ligation is the period in which serum bile acids and bilirubin levels reach the peak of elevation. We therefore postulate that the peak of elevation of bile acids and bilirubin can also trigger PKC activation. This PKC activation may cause the phosphorylation of caveolin-2, which may induce internalization of caveolae with OAT1 protein anchored with caveolin as has been recently suggested by Kwak et. al. [42]. This OAT1 downregulation (30%) was associated with a concomitant decrease of renal and systemic PAH clearance (40% and 30% respectively). The medium PAH plasma concentrations reached during the renal clearance infusion studies were 295 μM and 376 μM for the Sham and BDL rats respectively. The OAT1 mediated uptake of PAH is saturable with apparent Michaelis constants ranging 15 to 70 μM for rat OAT1 [13]. Therefore, PAH concentrations that we obtained in our "in vivo" experiments were sufficiently higher than the reported Km of rat OAT1. The diminished secreted load of PAH measured under saturating conditions was in part account for the lower number of OAT1 protein units observed, by immunoblot technique, in basolateral plasma membranes from BDL kidneys. The opposite was observed in the early phase of extrahepatic cholestasis where an increase of 30% of OAT1 abundance was associated with a similar increase in PAH clearance [22]. The differences observed in OAT1 abundance between 21 and 72 h of bile duct ligation remain to be explained. The increased OAT1 abundance observed in the early phase of extrahepatic cholestasis suggests a transient up-regulation similar to those described for renal OCT1 in cholestatic rats [43]. Maybe, different levels of various cytokines and growth factors which may affect gene transcription might be involved [44].

In contrast with OAT1, OAT3 expression increased both in homogenates and BLM from BDL kidneys. OAT3 is found in various cells and in all parts of the nephron, whereas OAT1 is confined to proximal tubules. The human and rat OAT3 transport PAH with relatively high affinity (87 and 65 μM respectively) [14,45], similarly to OAT1. On the contrary, estrone sulfate, cholate, and taurocholate are substrates for OAT3 and not for OAT1 as it has been demonstrated using *Xenopus laevis* oocytes [12,14,45,46], MDCK cells [47] and OAT3 knockout mice [48]. It is therefore possible that the over-expression of OAT3 does not compensate for the down-regulation of OAT1 regarding PAH transport because in this pathology the high plasma levels of bile acids might compete with PAH for OAT3 transport. Moreover, bile acids have been shown to regulate the expression of several genes involved in bile salt transport [49–51]. It is possible that high bile acids levels up-regulate OAT3 expression without affecting the OAT1 expression, being this another example of substrate specific regulation. The up-regulation of OAT3 protein in rat kidney in the present study is thus consistent with the adaptation to increased plasma bile acid levels that result from obstructive cholestasis, thus providing an additional alternative pathway for bile salt elimination.

MRP2 up-regulation has been described in the kidneys from rats with bile duct obstruction of 1 and 3 days [18,19]. On the other hand, renal MRP4 was down-regulated at 3 days after biliary obstruction [21]. Therefore, the protein expression of the luminal (MRP2 and MRP4) and basolateral organic anions renal transporters (OAT1 and OAT3), which all transport PAH, are differently regulated in extrahepatic biliary obstruction, thus indicating that different roles are played by these transporters in the pathogenesis of cholestasis. Tubular secretion is a vectorial transcellular transport system consisting of basolateral entry into the epithelial cells and secretion across the brush border membranes. Defects in either of

these two processes should therefore influence the tubular secretion of ionic drugs. In the present study, the tubular secretion of PAH was markedly reduced, thus suggesting a predominant role of OAT1 in this process.

It is important to mention that to predict the efficacy of a drug in vivo, it is critical to account for plasma protein binding because it determines the availability of the free drug, its half-life, and its subsequent renal elimination. Bow et al. [52] recently demonstrated that the degree of binding affinity for albumin to substrate determines whether or not a compound is actively secreted or reabsorbed by organic anion transporters. The common high unbound fraction of PAH increased from 95% in Sham rats to 100% in BDL rats. Since the bile acids and bilirubin plasma levels significantly increased in this experimental model, hence the binding sites on albumin for such hydrophobic anions might thus be occupied in the jaundiced rat, thereby increasing even more the unbound fraction of PAH.

The increase in the unbound fraction of PAH in BDL rats did not modify the distribution volumes of this anion. Nevertheless, in BDL rats there is a higher free concentration of PAH available for organic anion transporters, the OAT1 downregulation leads to a decrease in renal and systemic PAH clearance, thereby again stressing the main role of OAT1 in PAH excretion.

The present study stresses, once more, the important role of OAT1 expression in the renal elimination of PAH, independently of renal OAT3 expression. In this connection, it has been reported that a decrease of OAT1 abundance in BLM is associated with a decrease in PAH renal elimination in chronic renal failure [30], in obstructive nephropathy [28,29] and in response to 3 days of bile duct ligation, as it is shown in the present study. Meanwhile, OAT3 abundance in renal BLM has not changed, decreased or increased, respectively, in these three experimental models of pathologies [28–30]. Moreover, the increased renal excretion of PAH and furosemide is concomitantly observed with an increase in OAT1 and no changes in OAT3 abundance in BLM from rats with an early stage of extrahepatic cholestasis [22,53]. Accordingly, Eraly et al. [54] recently reported, using the OAT1 knock out mouse model, that regardless of the potential contribution of OAT3, the bulk of organic anion transport during the basolateral uptake step of the classical pathway is mediated by OAT1.

As highly accumulated anionic drugs observed during cholestasis may cause general body deterioration, the molecular mechanism(s) involved in the differential renal regulation of MRP2, MRP4, OAT3 and OAT1 expression should therefore be elucidated to prevent the occurrence of drug-induced toxicity due to this pathology.

Acknowledgements

This study was supported by the following grants: FONCYT and CONICET. The authors thank to Prof. Juan C. Picena (Cátedra de Anatomía y Fisiología Patológicas, Facultad de Ciencias Médicas, U.N.R.) and to Mrs, Alejandra Martínez (Facultad de Ciencias Bioquímicas y Farmacéuticas, U.N.R.) for their contribution to the histological studies. The authors also thank Wiener Lab Argentina for analytical kits. AMT was recipient of a travel grant from CONICET/JSPS (Japan Society for the Promotion of Science).

References

[1] N.R. Koopen, M. Müller, R.J. Vonk, P. Zimniak, F. Kuipers, Molecular mechanisms of cholestasis: causes and consequences of impaired bile formation, Biochim. Biophys. Acta 1408 (1998) 1–17.
[2] J. Reichen, F.R. Simon, Cholestasis, in: M. Arias, W.B. Jakoby, H. Popper, D. Schachter, D.A. Shafritz (Eds.), The Liver: Biology and Pathobiology, 2nd ed., Raven Press, New York, 1988, pp. 1105–1124.
[3] H.J. Kramer, Impaired renal function in obstructive jaundice: roles of the thromboxane and endothelin systems, Nephron 77 (1997) 1–12.
[4] M. Wójcicki, M. Drozdzik, T. Sulikowski, J. Wójcicki, B. Gawronska-Szklarz, S. Zielinski, L. Rózewicka, Pharmacokinetics of intravenously administered digoxin and histopathological picture in rabbits with experimental bile duct obstruction, Eur. J. Pharm. Sci. 11 (2000) 215–222.
[5] Ch. Fleck, H. Bräunlich, Interrelationships between excretion of drugs via urine and bile, Prog. Pharmacol. Clin. Pharmacol. 8 (1991) 511–529.
[6] M. Orellana, R. Rodrigo, L. Thielemann, V. Guajardo, Bile duct ligation and oxidative stress in the rat: effects in liver and kidney, Comp. Biochem. Physiol., Part C Pharmacol. Toxicol. 126 (2000) 105–111.
[7] S. Holt, R. Marley, B. Fernando, D. Harry, R. Anand, D. Goodier, K. Moore, Acute cholestasis-induced renal failure: effects of antioxidants and ligands for the thromboxane A2 receptor, Kidney Int. 55 (1999) 271–277.
[8] R. Talbert, Drug dosing in renal insufficiency, J. Clin. Pharmacol. 34 (1994) 99–110.
[9] N. Anzai, P. Jutabha, Y. Kanai, H. Endou, Integrated physiology of proximal tubular organic anion transport, Curr. Opin. Nephrol. Hypertens. 14 (2005) 472–479.
[10] T. Sekine, H. Miyazaki, H. Endou, Molecular physiology of renal organic anion transporters, Am. J. Physiol. 290 (2006) F251–F261.
[11] S.H. Wright, W.H. Dantzler, Molecular and cellular physiology of renal organic cation and anion transport, Physiol. Rev. 84 (2004) 987–1049.
[12] D.H. Sweet, L.M.S. Chan, R. Walden, X. Yang, D.S. Miller, J.B. Pritchard, Organic anion transporter 3 (Slc22a8) is a dicarboxylate exchanger indirectly coupled to the Na gradient, Am. J. Physiol. 284 (2003) F763–F769.
[13] T. Sekine, N. Watanabe, M. Hosoyamada, Y. Kanai, H. Endou, Expression cloning and characterization of a novel multispecific organic anions transporter, J. Biol. Chem. 272 (1997) 18526–18529.
[14] S.H. Cha, T. Sekine, J.-I. Fukushima, Y. Kanai, Y. Kobayashi, T. Goya, H. Endou, Identification and characterization of human organic anion transporter 3 expressing predominantly in the kidney, Mol. Pharmacol. 59 (2001) 1277–1286.
[15] R. Kojima, T. Sekine, M. Kawachi, S.H. Cha, Y. Suzuki, H. Endou, Immunolocalization of multispecific organic anion transporters, OAT1, OAT2, and OAT3, in rat kidney, J. Am. Soc. Nephrol. 13 (2002) 848–857.
[16] I. Leier, J. Hummel-Eisenbeiss, Y. Cui, D. Keppler, ATP-dependent para-aminohippurate transport by apical multidrug resistance protein MRP2, Kidney Int. 57 (2000) 1636–1642.
[17] P.H. Smeets, R.A. van Aubel, A.C. Wouterse, J.J. van den Heuvel, F.G. Russel, Contribution of multidrug resistance protein 2 (MRP2/ABCC2) to the renal excretion of p-aminohippurate (PAH) and identification of MRP4 (ABCC4) as a novel PAH transporter, J. Am. Soc. Nephrol. 15 (2004) 2828–2835.
[18] Y. Tanaka, Y. Kobayashi, E.C. Gabazza, K. Higuchi, T. Kamisako, M. Kuroda, K. Takeuchi, M. Iwasa, M. Kaito, Y. Adachi, Increased renal expression of bilirubin glucuronide transporters in a rat model of obstructive jaundice, Am. J. Physiol. 282 (2002) G656–G662.
[19] J. Lee, F. Azzaroli, L. Wang, C.J. Soroka, A. Gigliozzi, K.D.R. Setchell, W. Kramer, J.L. Boyer, Adaptive regulation of bile salt transporters in kidney and liver in obstructive cholestasis in the rat, Gastroenterology 121 (2001) 1473–1484.
[20] Q.-L. Pei, Y. Kobayashi, Y. Tanaka, Y. Taguchi, K. Higuchi, M. Kaito, N. Ma, R. Semba, T. Kamisako, Y. Adachi, Increased expression of multidrug resistance-associated protein 1 (mrp1) in hepatocyte basolateral membrane and renal tubular epithelia after bile duct ligation in rats, Hepatol. Res. 22 (2002) 58–64.

[21] G.U. Denk, C.J. Soroka, Y. Takeyama, W.-S. Chen, J.D. Schuetz, J.L. Boyer, Multidrug resistance-associated protein 4 is up-regulated in liver but down-regulated in kidneys in obstructive cholestasis in the rat, J. Hepatol. 40 (2004) 585–591.
[22] A. Brandoni, N.B. Quaglia, A.M. Torres, Compensation increase in organic anion excretion in rats with acute biliary obstruction: Role of the renal organic anion transporter 1, Pharmacology 68 (2003) 57–63.
[23] National Institutes of Health, Guide for Care and Use of Laboratory Animals, Publication 86-23, National Institutes of Health, Bethesda, 1985.
[24] J.A. Cerrutti, N.B. Quaglia, A.M. Torres, Characterization of the mechanisms involved in the gender differences in p-aminohippurate renal elimination in rats, Can. J. Physiol. Pharm. 79 (2001) 805–813.
[25] R. Shumaker, A basic interactive computer program for statistical and pharmacokinetic analysis of data, Drug Metab. Rev. 17 (1986) 331–348.
[26] H. Motulsky, Using nonlinear regression to fit curves, in: H. Motulsky (Ed.), Intuitive Biostatistics, Oxford University Press, New York, 1995, pp. 227–283.
[27] W.H. Waugh, P.T. Beall, Simplified measurement of PAH and other arylamines in plasma and urine, Kidney Int. 5 (1974) 429–432.
[28] S.R. Villar, A. Brandoni, N.B. Quaglia, A.M. Torres, Renal elimination of organic anions in rats with bilateral ureteral obstruction, Biochim. Biophys. Acta 1688 (2004) 204–209.
[29] S.R. Villar, A. Brandoni, N. Anzai, H. Endou, A.M. Torres, Altered expression of rat renal cortical OAT1 and OAT3 in response to bilateral ureteral obstruction, Kidney Int. 68 (2005) 2704–2713.
[30] A.M. Torres, M. Mac Laughlin, A. Muller, A. Brandoni, N. Anzai, H. Endou, Altered renal elimination of organic anions in rats with chronic renal failure, Biochim. Biophys. Acta 1740 (2005) 29–37.
[31] N.B. Quaglia, A. Brandoni, A. Ferri, A.M. Torres, Early manifestation of nephropathy in rats with arterial calcinosis, Renal Failure 25 (2003) 355–366.
[32] H.H. Roe, A photometric method for determination of inulin in plasma and urine, J. Biol. Chem. 178 (1949) 839–844.
[33] R.E. Jensen, W.O. Berndt, Epinephrine and norephinephrine enhance p-aminohippurate transport into basolateral membrane vesicles, J. Pharmacol. Exp. Ther. 244 (1988) 543–549.
[34] J.J. Sedmak, S.E. Grossberg, A rapid, sensitive and versatile assay for protein using Coomassie Brilliant Blue G250, Anal. Biochem. 79 (1977) 544–552.
[35] G.R. Wilkinson, Clearance approaches in pharmacology, Pharmacol. Rev. 39 (1987) 1–47.
[36] R. Lu, B.S. Chan, V.L. Schuster, Cloning of the human kidney PAH transporter: Narrow substrate specificity and regulation by protein kinase C, Am. J. Physiol. 276 (1999) F295–F303.
[37] G. You, K. Kuze, R.A. Kohanski, K. Amsler, S. Henderson, Regulation of mOAT-mediated organic anion transport by okadaic acid and protein kinase C in LLC-PK1 cells, J. Biol. Chem. 275 (2000) 10278–10284.
[38] N.A. Wolff, K. Thies, N. Kuhnke, G. Reid, B. Friedrich, F. Lang, G. Burckhardt, Protein kinase C activation downregulates human organic anion transporter 1-mediated transport through carrier internalization, J. Am. Soc. Nephrol. 14 (2003) 1959–1968.
[39] Z. Karim, N. Defontaine, M. Paillard, J. Poggioli, Protein kinase C isoforms in rat kidney proximal tubule: acute effect of angiotensin II, Am. J. Physiol. 269 (1995) C134–C140.
[40] Y.-P. Rao, R.T. Stravitz, Z.R. Vlahcevic, E.C. Gurley, J.J. Sando, P.B. Hylemon, Activation of protein kinase C α and δ by bile acids: correlation with bile acid structure and diacylglycerol formation, J. Lipid Res. 38 (1997) 2446–2454.
[41] Y. Hirohata, M. Fujii, Y. Okabayashi, Y. Nagashio, M. Tashiro, I. Imoto, T. Akiyama, M. Otsuki, Stimulatory effects of bilirubin on amylase release from isolated rat pancreatic acini, Am. J. Physiol. 282 (2002) 242–256.
[42] J.O. Kwak, H.-W. Kim, K.-J. Oh, D.S. Kim, K.O. Han, S.H. Cha, Co-localization and interaction of organic anion transporter 1 with caveolin-2 in the kidney, Exp. Mol. Med. 37 (2005) 204–212.
[43] G.U. Denk, C.J. Soroka, A. Mennone, H. Koepsell, U. Beuers, J.L. Boyer, Down-regulation of the organic cation transporter 1 of rat liver in obstructive cholestasis, Hepatology 39 (2004) 1382–1389.
[44] L.A. Denson, A. Bohan, M.A. Held, J.L. Boyer, Organ-specific alterations in RARα:RXRα abundance regulate rat Mrp2 (Abcc2) expression in obstructive cholestasis, Gastroenterology 123 (2002) 599–607.
[45] H. Kusuhara, T. Sekine, N. Utsunomiya-Tate, M. Tsuda, R. Kojima, S.H. Cha, Y. Sugiyama, Y. Kanai, H. Endou, Molecular cloning and characterization of a new multispecific organic anion transporter from rat brain, J. Biol. Chem. 19 (1999) 13675–13680.
[46] Y. Uwai, M. Okuda, K. Takami, Y. Hashimoto, K. Inui, Functional characterization of the rat multispecific organic anion transporter OAT1 mediating basolateral uptake of anionic drugs in the kidney, FEBS Lett. 438 (1998) 321–324.
[47] A. Aslamkhan, U.-H. Han, R. Walden, D.H. Sweet, J.B. Pritchard, Stoichiometry of organic anion/dicarboxylate exchange in membrane vesicles from rat renal cortex and hOAT1-expressing cells, Am. J. Physiol. 285 (2003) F775–F783.
[48] D.H. Sweet, D.S. Miller, J.B. Pritchard, Y. Fujiwara, D.R. Beier, S.K. Nigam, Impaired organic anion transport in kidney and choroid plexus of organic anion transporter 3 (Oat3 (Slc22a8)) knockout mice, J. Biol. Chem. 30 (2002) 26934–26943.
[49] D. Rost, T. Herrmann, P. Sauer, H.-L. Schmidts, B. Stieger, P.J. Meier, W. Stremmel, A. Stiehl, Regulation of rat organic anion transporters in bile salt-induced cholestatic hepatitis: effect of ursodeoxycolate, Hepatology 38 (2003) 187–195.
[50] D. Jung, M. Podvinec, U.A. Meyer, D.J. Mangelsdorf, M. Fried, P.J. Meier, G.A. Kullak-Ublick, Human organic anion transporting polypeptide 8 promoter is transactivated by the farnesoid X receptor/bile acid receptor, Gastroenterology 122 (2002) 1954–1966.
[51] J.L. Boyer, M. Trauner, A. Mennone, C.J. Soroka, S.-Y. Cai, T. Moustafa, G. Zollner, J.Y. Lee, N. Ballatori, Up-regulation of a basolateral FXR-dependent bile acid efflux transporter, OSTα-OSTβ, in cholestasis in humans and rodents, Am. J. Physiol. 290 (2006) G1124–G1130.
[52] D.A. Bow, J.L. Perry, J.D. Simon, J.B. Pritchard, The impact of plasma protein binding on the renal transport of organic anions, J. Pharmacol. Exp. Ther. 316 (2006) 349–355.
[53] A. Brandoni, S.R. Villar, J.C. Picena, N. Anzai, H. Endou, A.M. Torres, Expression of rat renal cortical OAT1 and OAT3 in response to acute biliary obstruction, Hepatology 43 (2006) 1092–1100.
[54] S.A. Eraly, V. Vallon, D.A. Vaughn, J.A. Gangoiti, K. Richter, M. Nagle, J.C. Monte, T. Rieg, D.M. Truong, J.M. Long, B.A. Barshop, G. Kaler, S.K. Nigam, Decrease renal organic anion secretion and plasma accumulation of endogenous organic anions in OAT1 knock-out mice, J. Biol. Chem. 281 (2006) 5072–5083.

J. Biochem. 139, 761–769 (2006)
doi:10.1093/jb/mvj079

Amino Acids C-Terminal to the 14-3-3 Binding Motif in CDC25B Affect the Efficiency of 14-3-3 Binding

Sanae Uchida[1], Akitsugu Kubo[1], Ryoichi Kizu[2,*], Hitoshi Nakagama[3], Tsukasa Matsunaga[1], Yukihito Ishizaka[4] and Katsumi Yamashita[1,5]

[1]Division of Life Science and [2]Division of Environmental Science and Engineering, Graduate School of Science and Technology, Kanazawa University, Kakuma-machi, Kanazawa, Ishikawa 920-1192; [3]Biochemistry Division, National Cancer Center Research Institute, 1-1 Tsukiji 5-chome, Chuo-ku, Tokyo 104-0045; [4]Division of Intractable Disease, International Medical Center of Japan, 21-1 Toyama 1-chome, Shinjyuku-ku, Tokyo 162-8655; and [5]Cancer Research Institute, Kanazawa University, 13-1 Takara-machi, Kanazawa, Ishikawa 920-0934

Received February 8, 2006; accepted February 21, 2006

The phospho-site adapter protein 14-3-3 binds to target proteins at amino acid sequences matching the consensus motif Arg-X-X-Ser/Thr-X-Pro, where the serine or threonine residue is phosphorylated and X is any amino acid. The dual-specificity phosphatase CDC25B, which is involved in cell cycle regulation, contains five 14-3-3 binding motifs, but 14-3-3 preferentially binds to the motif at Ser309 in CDC25B1 (or Ser323 in CDC25B3). In the present study, we demonstrate that amino acid residues C-terminal to the 14-3-3 binding motif strongly affect the efficiency of 14-3-3 binding. Alanine substitutions at residues downstream of the Ser309 motif dramatically reduced 14-3-3 binding, although phosphorylation of Ser309 was unaffected. We also observed that binding of endogenous 14-3-3 to mutant CDC25B occurred less efficiently than to the wild type. Mutants to which 14-3-3 cannot bind efficiently tend to be located in the nucleus, although not as specifically as the alanine substitution mutant of Ser309. These results indicate that amino acid sequences C-terminal to the consensus binding site have an important role in the efficient binding of 14-3-3 to at least CDC25B, which may partly explain why some consensus sequences are inactive as 14-3-3 binding sites.

Key words: 14-3-3, CDC25B, cell cycle, phosphorylation, subcellular localization.

Abbreviations: CDK, cyclin-dependent kinase; GST, glutathione-S-transferase; MAPKAP, mitogen-activated protein kinase–activated protein; MK2, MAPKAP kinase 2; NLS, nuclear localization signal.

The eukaryotic cell cycle progresses through successive cycles of activation and inactivation of cyclin-dependent kinases (CDKs) that are complexed with cyclins. The activities of these complexes are regulated via several mechanisms, including inhibition of CDK by small proteins (*e.g.*, p16, p21, and p27), inhibitory phosphorylation by Wee1/Myt1 kinases at the ATP binding site of CDK, and activation of dephosphorylation by CDC25 dual-specificity phosphatases.

Three CDC25 phosphatases have been identified in mammalian cells, CDC25A, CDC25B, and CDC25C (*1*). The first CDC25 phosphatase gene to be identified was that encoding CDC25C, which dephosphorylates phospho-Tyr15 of CDK1 (previously phosphorylated by Wee1 kinase) to promote the G2 to M phase transition (*2*, *3*). Studies using cultured mammalian cells have suggested that CDC25A plays a role in the G1 to S phase transition by activating CDK2/cyclin E (*4*, *5*), and that CDC25B and CDC25C function in M phase entry by activating and maintaining CDK1:cyclin B activity during the M phase (*6–9*).

*To whom correspondence should be addressed at the present address: Department of Environmental Biochemistry, Faculty of Pharmaceutical Sciences, Doshisha Women's College of Liberal Arts, Kodo, Kyotanabe 610-0395. Tel: +81 76 264 5809, Fax: +81 76 264 5989, E-mail: katsumi@kenroku.kanazawa-u.ac.jp

Recent reports provided evidence that CDC25A also plays an important role in the G2 to M phase transition, thus indicating that CDC25A regulates all cell cycle stages (*10*, *11*). However, mice depleted of CDC25C by gene targeting develop normally and become fertile adults (*12*), and CDC25B knockout mice are born essentially healthy, although the females are sterile because of a defect in oogenesis (*13*). A recent report confirmed that mice lacking both the CDC25B and CDC25C genes are born healthy and that cells derived from these mice not only undergo normal entry to the M phase but also exhibit no checkpoint defects (*14*). Therefore, CDC25B and CDC25C are not essential for mouse development and for DNA damage checkpoints.

CDC25 proteins are CDK activators and, as a result, may comprise important cell cycle checkpoints (*15–17*). When the cell cycle checkpoint kinase CHK1 or CHK2 is activated by genotoxic stress, it phosphorylates several serine or threonine residues in CDC25A, which leads to the ubiquitin-proteasome pathway-mediated degradation of CDC25A that accompanies cell cycle arrest at the G1, G2, or intra-S phase (*10*, *17*). CDC25B and CDC25C, as well as CDC25A, are good substrates for CHK1 and CHK2 *in vitro* (*18–20*). CDC25B overexpression overrides the G2 checkpoint after ionizing radiation and other genotoxic stresses, and overproduction of a non-phosphorylated

mutant form of CDC25C partially overrides the G2 checkpoint (*21–24*).

One of the phospho-site adapter proteins, 14-3-3, appears to be centrally involved in the CDC25 function, especially in terms of checkpoint function (*15, 22–25*). CHK1 and CHK2 [and very recently mitogen-activated protein kinase-activated protein (MAPKAP) kinase 2 (MK2)] have been shown to phosphorylate CDC25B and CDC25C at phosphorylation sites containing the 14-3-3 consensus binding sequence (*23, 24, 26*). The binding of 14-3-3 to CDC25B or CDC25C may recruit these phosphatases to the cytoplasm from the nucleus and help to retain them there, thus preventing CDK1 activation in the nucleus (*27–30*). However, CDC25 phosphorylation by CHK1 or CHK2 down-regulates its phosphatase activity, in both 14-3-3 binding–dependent and –independent manners (*31–33*). At this point, the precise role of CDC25 binding to 14-3-3 in the normal cell cycle and its checkpoints remains to be defined.

We previously reported that 14-3-3β and 14-3-3ε can bind to Ser309 phosphorylation site in CDC25B1, and that the single phosphorylation at Ser309 is sufficient to sustain the binding of the β and ε 14-3-3 isoforms (*30*). In the present study, we further examined the importance of 14-3-3 binding in the regulation of CDC25B. We studied binding to CDC25B of other 14-3-3 isoforms, such as 14-3-3γ, η, θ, which is also called τ, and ζ and found that they bind primarily to the Ser309 site. Furthermore, our results reveal major roles not only for the amino acids in the Ser309 consensus site but also for the amino acids surrounding the consensus site in efficient 14-3-3 binding.

EXPERIMENTAL PROCEDURES

Cell Culture and Transformation—HEK293, Cos-7, and HeLa cells (American Type Culture Collection strains CRL-1573, CRL-1651, and CCL-2, respectively) were grown in Dulbecco's Modified Eagle's Medium supplemented with 10% fetal bovine serum, 100 μg/ml penicillin, 100 U/ml streptomycin, and 50 μg/ml M-Plasmocin under a humidified atmosphere of 5% CO_2. Fetal bovine serum, penicillin, and streptomycin were from Sigma (St. Louis, MO, USA), and M-Plasmocin from Invivogen (San Diego, CA, USA). For the transformation of HEK-293 and Cos-7 cells, appropriate amounts of DNA were transfected with FuGENE6 (Roche Diagnostics, Indianapolis, IN, USA). HeLa cells were transfected with LipofectAMINE2000 (Invitrogen, Carlsbad, CA, USA) according to the manufacturer's recommendation.

Plasmid Construction—Plasmids encoding N-terminal double FLAG-tagged CDC25B1, and N-terminal double myc-tagged 14-3-3β, ε, and σ were constructed as described previously (*30*). For the isolation of the other 14-3-3 subtypes, the coding regions were amplified by PCR using specific primers for 14-3-3γ, η, θ, and ζ. Each amplified fragment was subcloned into a modified pEF6-mycHisB vector (Invitrogen) such that a double Myc-tag was encoded at each N-terminus. The sequences of these primers are shown in Table 1. Human CHK1 and CHK2 were provided by Steve Elledge of Harvard Medical School. Human MK2 cDNA was purchased from Open Biosystems (Huntsville, AL, USA). All were amplified with specific primers (Table 1) and subcloned into modified pEF6-mycHisB such that a double HA tag was encoded at the N- or C-terminus and a 6×His tag was encoded at the C-terminus. The GST-CDC25B peptide expression plasmid was constructed by PCR amplification of the CDC25B gene, digestion of the PCR product with *Nco*I and *Xho*I, and ligation into the pGEX-KG vector (*34*). The primers used to amplify CDC25B are shown in Table 1.

Site-Directed Mutagenesis—PCR-based site-directed mutagenesis with complementary oligonucleotide pairs was used to insert alanine point mutations in CDC25B, and to place a *Bam*HI restriction site between Leu319 and Lys320 of CDC25B. The sequence of one strand of each primer pair is shown in Table 2.

Antibodies—Antisera against a phospho-Ser309 peptide (*23*) and the FLAG tag (*35*) were raised as described and affinity purified. Anti-myc and anti-HA antibodies were from Cell Signaling (Beverly, MA, USA), anti-GST

Table 1. **PCR primers used for amplification and construction of tagged proteins.**

Gene	Primer	DNA sequence (5′→3′)
14-3-3γ	Forward	AGCCCCGGATCCATGGTGGACCGCGAGCAACTGGTG
	Reverse	TCCCCTGAATTCTTAATTGTTGCCTTCGCCGCCATC
14-3-3η	Forward	CCGAGCCGGATCCCATATGGGGGACCGGGAGCAGCTGCTG
	Reverse	CCTGAAGAATTCTCAGTTGCCTTCTCCTGCTTCTTC
14-3-3θ	Forward	CCCGCGGGATCCATGGAGAAGACTGAGCTGATCCAG
	Reverse	ACACCCGAATTCGATTTAGTTTTCAGCCCCTTCTGC
14-3-3ζ	Forward	GAACATGGATCCATGGATAAAAAATGAGCTGGTTCAG
	Reverse	AAGTTGGAATTCCGGTTAATTTTCCCCTCCTTCTTC
CHK1	Forward	CTCGGTCTAGACATGGCAGTGCCCTTTGTG
	Reverse	GCCGATGGTGATATCATGTGGCAGGAAGCC
CHK2	Forward	GCTCACGGTACCGCCATGTCTCGGGAGTCG
	Reverse	TTCAAACCACGGGATATCCAACACAGCAGC
MK2	Forward	TCCCCGGGTACCATGCTGTCCAACTCCCAGGGCCAG
	Reverse	CGCGGTGATATCGTGGGCCAGAGCCGCAGCCTCCAGGG
MKK6	Forward	AAGGGGCATATGTCTCAGTCGAAAGGCAAGAAGCGAAACCCTGGC
	Reverse	GTCCACGATATCTTAGTCTCCAAGAATCAGTTTTACAAAAGATGC
GST-CDC25B	Forward	GTTCCCCCAGCCATGGAGAGTCTCATTAGT
	Reverse	TGATTTTGACTCGAGCTAGCGGGCTTTAGG

Table 2. **Sequences of primer pairs used for PCR-based site-directed mutagenesis of CDC25B.**

Mutation	Forward primer sequence (5′→3′)
Leu304Ala	AAGTGCCAGCGGGCCTTCCGCTCTCCG
Arg306Ala	CAGCGGCTCTTCGCCTCTCCGTCCATG
Ser309Ala	CTCTTCCGCTCTCCGGCCATGCCCTGCAGC
Met310Ala	CGCTCTCCGTCCGCCCCCTGCAGCGTG
Pro311Ala	TCTCCGTCCATGGCCTGCAGCGTGATC
Cys312Ala	CCGTCCATGCCCGCCAGCGTGATCCGG
Ser313Ala	TCCATGCCCTGCGCCGTGATCCGGCCC
Val314Ala	ATGCCCTGCAGCGCCATCCGGCCCATC
Ile315Ala	CCCTGCAGCGTGGCCCGGCCCATCCTC
Arg316Ala	TGCAGCGTGATCGCTCCCATCCTCAAG
Pro317Ala	AGCGTGATCCGGGCCATCCTCAAGAGG
Ile318Ala	GTGATCCGGCCCGCCCTCAAGAGGCTG
Leu319Ala	ATCCGGCCCATCGCCAAGAGGCTGGAG
319/BamHI/320	CGGCCCATCCTCGGATCCAAGAGGCTGGAG

serum from Amersham Biosciences (Piscataway, NJ, USA), and anti-FLAG M2-beads from Sigma.

Preparation of Cell Extracts, Immunoprecipitation, and Immunoblotting—Crude cell extracts were prepared as described previously (*30*). Cells were collected by scraping, washed in ice-cold phosphate-buffered saline (PBS), and lysed with immunoprecipitation (IP) buffer (50 mM Tris-HCl, pH 7.5, 150 mM NaCl, 0.5% NP-40, 5 mM EGTA, and 1 mM EDTA) supplemented with protease and phosphatase inhibitor mixes as described previously (*30*). Cell extracts were centrifuged at 15,000 ×*g* for 10 min at 4°C, the supernatant fractions were collected, and the protein concentrations were determined by the Bradford method (Bio-Rad, Richmond, CA, USA) (*36*). For immunoprecipitation, typically 500 μg of protein was mixed with anti-FLAG M2-agarose beads or 2 μg of anti-myc monoclonal antibodies followed by protein G-Sepharose beads (Amersham Biosciences). Crude cell extracts or immunoprecipitates were subjected to immunoblotting using rabbit polyclonal anti-FLAG antibodies (for CDC25B), mouse monoclonal anti-myc antibodies (for 14-3-3), or mouse monoclonal anti-HA antibodies (for kinases).

Protein Purification—Protein kinases were prepared from cDNA-transfected Cos-7 cells. Typically, 8×10^5 Cos-7 cells in a 6-cm dish received 4 μg of plasmid DNA with FuGENE6. After 24 h, the cells were collected, washed with PBS, and lysed with EDTA-free IP buffer supplemented with a 1:100 dilution of FOCUS Protease Arrest (EMD Biosciences, San Diego, CA, USA), 20 mM *p*-nitrophenyl phosphate, 20 mM NaF, and 20 mM β-glycerophosphate. To purify the kinases, Ni^{2+}-charged immobilized metal-chelating Sepharose beads (Amersham Biosciences) were added to the cell extracts containing 1.5 mg protein, and the protein-bound beads were used directly in kinase assays. GST-tagged proteins were expressed in *Escherichia coli* BL21 (DE3) cells transformed with the appropriate cDNA plasmid constructs. Expression was induced with 0.4 mM isopropyl-β-D-thiogalactopyranoside, and proteins were purified with glutathione–Sepharose beads (Amersham Biosciences).

Indirect Immunofluorescence Microscopy—Indirect immunofluorescence analysis was performed as described previously (*30*, *37*). Transfected HEK293 cells were fixed with 3.7% formaldehyde and then permeabilized with 0.5% Triton X-100. Expressed CDC25B proteins were detected with rabbit polyclonal anti-FLAG antibodies, followed by AlexaFluor 594– or 488–conjugated goat anti-rabbit IgG (Molecular Probes, Eugene, OR, USA), and expressed 14-3-3 was detected with mouse monoclonal anti-Myc antibodies and AlexaFluor 488–conjugated goat anti-mouse IgG. Nuclei were stained with 4′,6-diamino-2-phenylindole (Sigma).

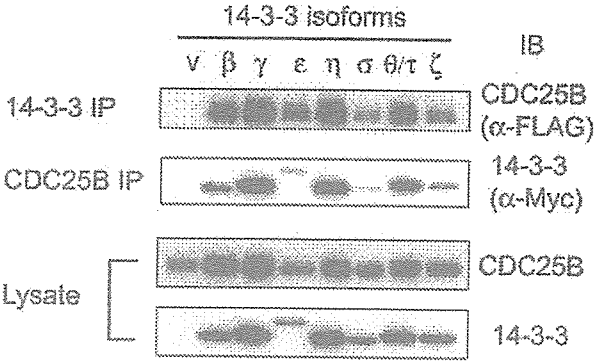

Fig. 1. **Binding of 14-3-3 subtypes to CDC25B.** HEK293 cells (1.4×10^6 cells per 35-mm plate) were transfected with 3 μg of FLAG-tagged CDC25B DNA and 0.6 μg of myc-tagged 14-3-3 DNA. The cells were collected 24 h after transfection, and cell extracts were prepared. The cell extracts were either subjected to Western blotting to visualize protein expression or further processed for immunoprecipitation with anti-FLAG or anti-myc antibodies to analyze binding. Upper panel: IP with anti-myc (14-3-3), followed by IB with anti-FLAG (CDC25B); second panel: IP with anti-FLAG (CDC25B), followed by IB with anti-myc (14-3-3).

RESULTS

All Seven Isoforms of 14-3-3 Bind to CDC25B—We previously showed that 14-3-3 isoforms β, ε, and σ bind efficiently to CDC25B, with the β and ε isoforms binding preferentially to the 14-3-3 binding motif at Ser309 (309 site), and the σ isoform binding preferentially to the motif at Ser216 (216 site) (*30*). In the present study, we analyzed the binding properties of four additional isoforms of 14-3-3. The genes for the γ, η, θ, and ζ isoforms were amplified by PCR and expressed in HEK293 cells. Each 14-3-3 isoform was co-expressed with CDC25B, isolated, and analyzed as to its interaction with CDC25B. As shown in Fig. 1, all the14-3-3 isoforms were able to interact with CDC25B. CDC25B was detected in immunoprecipitates of all the 14-3-3 isoforms (Fig. 1, upper panel), and all the 14-3-3 isoforms were recovered in the CDC25B co-immunoprecipitates (Fig. 1, second panel). Taking the protein expression levels into account, the 14-3-3ε, σ, and ζ isoforms appeared to bind more weakly to CDC25B than did the other 14-3-3 isoforms (Fig. 1, second and fourth panels).

As we reported previously (*30*), CDC25B has five 14-3-3 consensus binding motifs (Fig. 2A). Here, we examined the CDC25B binding site preference of each 14-3-3 isoform using co-transfection with plasmids encoding various CDC25B mutants. Five of these mutants contained

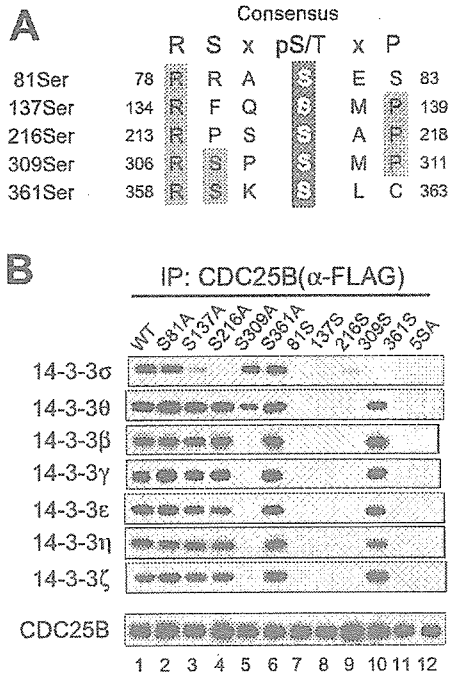

C

14-3-3 subtype	CDC25B mutants											
	WT	S61A	S137A	S216A	S309A	S361A	81S	137S	216S	309S	361S	5SA
σ	++	++	+	–	++	++	–	–	±	–	–	–
θ	++	++	++	++	+	++	–	–	–	++	–	–
β	++	++	++	++	–	++	–	–	–	++	–	–
γ	++	++	++	++	±	++	–	–	–	++	–	–
ε	++	++	++	++	±	++	–	–	–	++	–	–
η	++	++	++	++	–	++	–	–	–	++	–	–
ζ	++	++	++	++	±	++	–	–	–	++	–	–

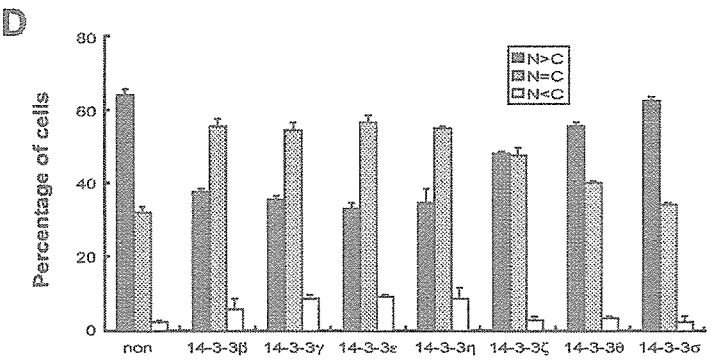

Fig. 2. **CDC25B binding site preferences of 14-3-3 subtypes.** FLAG-tagged CDC25B mutants with Ser→Ala substitutions at possible 14-3-3 binding sites (*30*) were co-transfected with each 14-3-3 subtype, as described in Fig. 1. Cell extracts were prepared 24 h after transfection and then immunoprecipitated with anti-FLAG-agarose beads to recover the CDC25B mutant proteins. Recovered CDC25B and co-immunoprecipitated 14-3-3 were detected by Western blotting. A: Possible 14-3-3 consensus binding sites and their amino acid sequences. B: Isoforms of 14-3-3 recovered with anti-FLAG-agarose beads. The bottom panel indicates a typical result of expression of co-transfected CDC25B mutants. C. Summary of the results shown in B. ++, strong signal; +, moderate signal; ±, discernible after long exposure; –, no signal. D. Subcellular localization of wild-type CDC25B upon co-expression with 14-3-3 subtypes. Cover slips in 35-mm plates were seeded with 2×10^6 HEK293 cells. After 2 days, the cells were transfected with myc-tagged 14-3-3 subtypes in combination with FLAG-tagged wild-type CDC25B. The cells were fixed 24 h after transfection, and the subcellular localization of CDC25B was determined by staining with anti-FLAG antibodies. More than 200 cells were examined. The data shown are the averages of three independent experiments. Bars = standard deviation.

single-site Ser→Ala substitutions in one 14-3-3 binding motif (*e.g.*, mutant Ser309Ala). In addition, the 309Ser mutant contained Ser→Ala substitutions at all possible binding sites except site 309, and the 5SerAla mutant contained Ser→Ala substitutions at all five putative binding sites.

CDC25B immunoprecipitates were recovered from cells co-transfected with the *14-3-3* and mutant *CDC25* genes, and 14-3-3 was detected on Western blots. All 14-3-3 isoforms except 14-3-3σ were found to bind preferentially to site 309 (Fig. 2B), as shown previously (*30*). Although substantial binding of 14-3-3θ to the Ser309Ala mutant did occur, comparison with the other single-site mutations revealed that 14-3-3θ bound preferentially to site 309. These results are summarized in Fig. 2C.

We examined the effect of co-transfection with 14-3-3 isoforms on the subcellular localization of CDC25B. Previously, we found that the binding of 14-3-3 at site 309 caused CDC25B to move from the nucleus to the cytoplasm (*30*). In the present study, we found that 14-3-3 isoforms that preferentially bound at site 309 caused CDC25B to be exported from the nucleus to the cytoplasm, and that isoforms that bound weakly or non-preferentially to site 309 did not have such an effect (Fig. 2D). The 14-3-3θ isoform, which binds preferentially to site 309, exhibited a mobilizing effect on the 309Ser mutant (data not shown), consistent with the results of the binding analysis above.

Mutations Near Ser309 of CDC25B Interfere with 14-3-3 binding—The effects of co-transfection with 14-3-3 on the cytoplasmic distribution of CDC25B indicated that 14-3-3 binding at site 309 may have masked the nuclear localization signal (NLS) sequence of CDC25B, which begins about ten residues downstream of the binding site (Fig. 3A). We therefore conducted experiments to determine the effect of an increased distance between Ser309 and the NLS sequence. Lys320 is the first residue of the bipartite NLS sequence in CDC25B. To enable the in-frame insertion of additional amino acids, we initially used mutagenesis to introduce a *Bam*HI site between residues 319 and 320. The *Bam*HI recognition sequence resulted in the insertion of Gly–Ser (GS) dipeptide immediately before Lys320 (Fig. 3A). We found, however, that this GS insertion abolished 14-3-3 binding to CDC25B, despite the fact that phosphorylation at site 309 was detected with phospho-Ser309 antibodies (Fig. 3B).

These results were intriguing because there have been no previous reports that amino acid sequences C-terminal

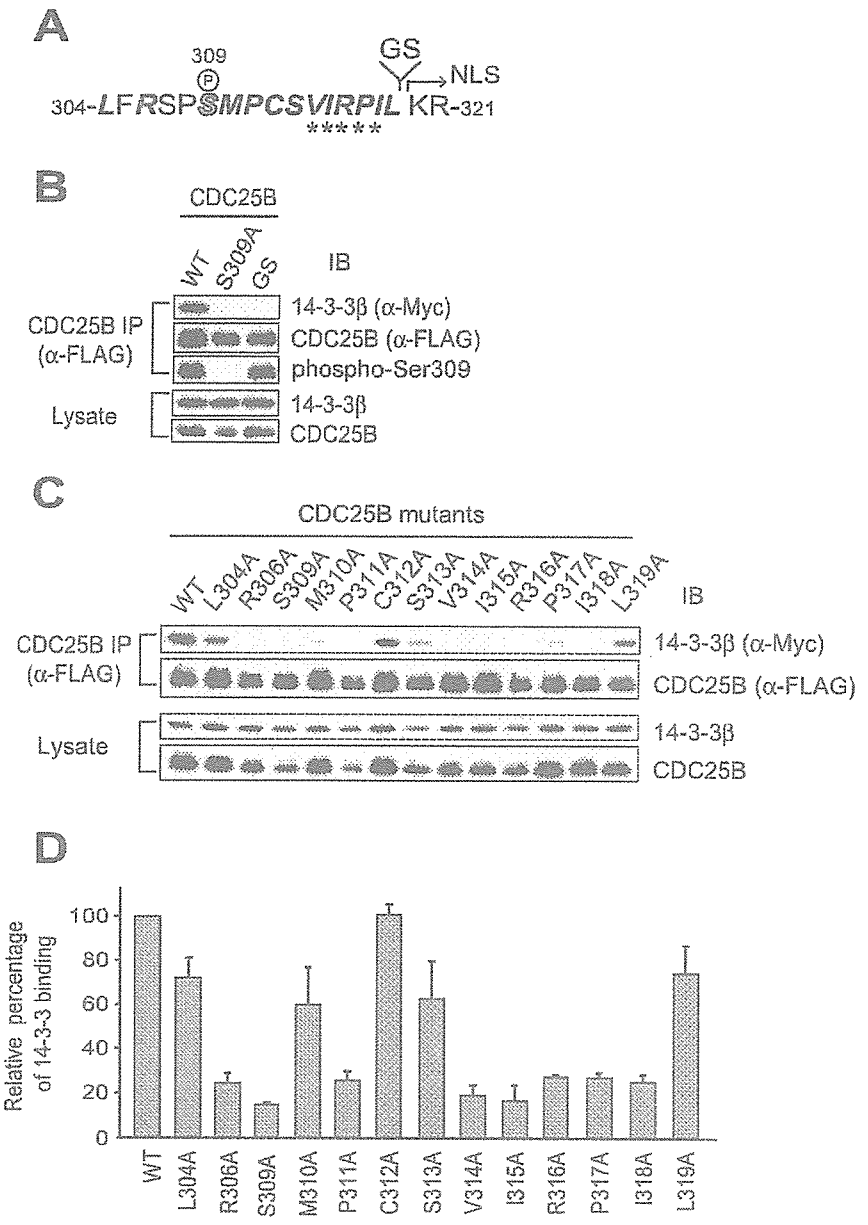

Fig. 3. **Binding of 14-3-3β to CDC25B mutants with substitutions near Ser309.** CDC25B mutants containing point substitutions near Ser309 were co-transfected with 14-3-3β, and CDC25B mutant proteins were isolated with anti-FLAG-agarose beads as described in Fig. 2. CDC25B-bound 14-3-3β was identified with an anti-myc antibody. A. Amino acid sequence from Leu304 to Arg321. Ser309 is denoted by an outlined letter S. A *Bam*HI site (GGATCC), which encodes Gly–Ser, was inserted between Leu319 and Lys320. Lys320 is the N-terminal end of the NLS sequence in CDC25B, which is indicated by an arrow. Bold italic letters indicate amino acids changed to Ala to analyze 14-3-3 binding, the results of which are depicted in (C) and (D). Asterisks indicate the hydrophobic amino acid stretch (see text). The GS insertion mutant (+ GS in B) and a series of point mutants (C) of CDC25B were analyzed as to their binding to 14-3-3β and the phosphorylation of Ser309, which was determined with anti-phospho-Ser309 antibodies. The efficiency of 14-3-3β binding to each CDC25B mutant relative to wild-type CDC25B was calculated from the data presented in (C) and is depicted in (D). The data shown are the averages of three independent experiments. Bars = standard deviation.

to the 14-3-3 binding site affect the interaction between 14-3-3 and its target proteins. We further examined this phenomenon by introducing single alanine point mutations at residues 304 to 319 of CDC25B, and then co-transfecting the resulting mutants and 14-3-3β (indicated by bold italic letters in Fig. 3A). Surprisingly, all of the tested point mutations except Cys312Ala and Leu319Ala caused a diminished interaction with 14-3-3 (Fig. 3C). The results clearly demonstrate that the hydrophobic amino acid region from Val315 to Ile318 seems to be important for 14-3-3 binding (Fig. 3D and depicted by asterisks in Fig. 3A). Pro311 of CDC25B, which is part of the 14-3-3 binding consensus sequence, also appeared to be important for 14-3-3 binding. Thus, alterations in the amino acids near the core consensus sequence of site 309 of CDC25B negatively affected its ability to bind to 14-3-3.

Ser309 Phosphorylation by Several Candidate Kinases—To study the *in vivo* phosphorylation of Ser309 in these mutants, we transfected some of the mutant *CDC25B* genes, and the mutant proteins were recovered and assayed for phosphorylation at Ser309. As shown in Fig. 4A, phosphorylation of Ser309 occurred in all of the mutants expressed in HEK293 cells, except for the Pro317Ala mutant expressed in Cos-7 cells.

Several kinases that phosphorylate Ser309 of CDC25B1 (or Ser323 of CDC25B3) have been reported. We attempted to determine which kinases could phosphorylate the CDC25B mutants. We expressed candidate kinases